Chapter 3: Historical and Projected Climate

Linda A. Joyce and Marian Talbert

Introduction

The Intermountain Adaptation Partnership (IAP) region is characterized by extreme temperatures and precipitation; it is home to some of the driest, hottest, and coldest locations in the conterminous United States. The region has numerous mountain ranges, high-elevation basins and valleys, and low-elevation mesas and canyons. Climate is influenced by this diverse and complex terrain. The IAP region is bounded on the eastern side by the Rocky Mountains and on the western side by the Sierra Nevada. For this region, moisture comes predominantly from the Pacific Ocean, and consequently much of the moisture occurs as orographic precipitation in the mountains.

This chapter provides a brief discussion of the current climate in each of the six subregions to set the context for projected changes in climate under two future scenarios. The Great Basin and Semi Desert, and the Intermountain Semi Desert subregions are warmer and drier than the Southern Greater Yellowstone and Middle Rockies subregions. The Plateaus, and Uintas and Wasatch Front subregions have intermediate amounts of precipitation. Within each subregion, climate influences the ecosystem services that forests and rangelands provide. Thus, an understanding of how climate may change in the future is vital for long-term planning and management.

This chapter focuses on the historical record of climate, primarily temperature and precipitation, and the projected changes in temperature and precipitation. Chapter 4 describes the effects of climate on hydrological processes, snowpack and glaciers, streamflow, sediment yield, and drought. The impacts of climate change on wildfire and geologic processes, such as mass wasting, are discussed in Chapter 8. Other chapters review literature on the effects of climate change on particular resources, such as individual species in Chapter 9.

Assessing Climate Futures for Natural Resource Management

Information on weather and climate are used to inform the decisionmaking process in natural resource management. Day-to-day resource management practices are implemented with information on real-time conditions of temperature, precipitation, wind, humidity, and other meteorological factors. These specific conditions over a relatively short time period and in a particular place are what we call weather. This information is used to make on-the-ground real-time decisions, such as the start of prescribed fire activities.

Long-term resource management strategies and plans are informed by the observed dynamics of precipitation, temperature, wind, snowfall, and other measures of weather over a long time period in a particular place. Climate is defined by this long-term meteorological information. Understanding the climate of an area assists managers in identifying both the general characteristics of the area and the risks associated with potential extremes of weather conditions, such as flooding, drought, wildfire, and extreme heat or cold events. Typically, the most recent three full decades (e.g., 1981–2010) are used to determine the normal climate, or the average conditions on an annual, monthly, or daily basis. Long-term records (>30 years) are also used to assess the risk of specific weather events and thresholds that have relevance to management, such as in the sizing of culverts and bridges.

Although long-term records of climate can help to establish the characteristics of the average climate or the probability of certain extreme events, future climate may be different than the past 30 to 60 years (Walsh et al. 2014). To understand how climate might change, scientists use global climate models (GCMs), which are supercomputer-based simulations that represent the key components, interactions, and feedback processes of the climate system, based on fundamental physical laws and decades of observations of the atmosphere, oceans, ice sheets, and biosphere. These models have been used to study the physical dynamics of the atmosphere and the interaction between the atmosphere and the surface of the Earth, as well as interactions with ocean currents moving heat around the globe. Information on future changes in climate provided by GCMs can be helpful in understanding how the environmental settings of plants, animals, and habitats may change in the future; how runoff and seasonal flows may vary with precipitation and timing of snowmelt; and how wildfire, insects and disease patterns may change.

Scenarios

Climate models have been an important part of the Intergovernmental Panel on Climate Change (IPCC) assessments since 1990. In 1995, atmospheric scientists came together to coordinate a standardized set of model runs (also called experiments) for evaluating changes to past and future global climate: the Coupled Model Intercomparison Project (CMIP) (Meehl et al. 2007). This project also developed a web portal where these GCM results could be archived and made available for use by other scientists. This approach allows for a rigorous comparison of results across the models because the models have similar initial conditions and similar changes in atmospheric chemistry and land use cover over time. This approach improves our understanding of the range of possible future climate change.

Many of the model experiments focus on improving the ability of the model to describe climate; however, these models can also be used to look at the evolution of climate over time when a description of how the future may develop is constructed. A climate scenario is a simplified representation of future climate, based on climatological relationships constructed for investigating the potential consequences of human-caused climate change (Stocker et al. 2013). Climate dynamics are influenced by land surface changes, such as building cities or changing land use from forest to agriculture, by the chemical composition of the atmosphere, and by human contributions to the atmosphere through land management, energy sources, and industrial processes. Constructing a scenario requires describing how these forces may develop over time. The goal of working with scenarios is to understand uncertainties and alternative conditions associated with climate change, thus informing decisions or options for a range of possible futures (IPCC Data Distribution Center 2016).

Climate scenarios in the last three IPCC assessments have been constructed in two ways (table 3.1). In the third and fourth IPCC assessments, scenario development started with specific assumptions about population growth, economic growth, and policies related to alternative energy and conventional fossil fuel sources; then the resultant greenhouse gas emissions to the atmosphere were projected (Solomon et al. 2007). These scenarios were called SRES scenarios, named for the report that developed them, the Special Report on Emission Scenarios (Nakićenović et al. 2000). These different combinations of population, economic growth, and energy policy resulted in scenarios that ranged from low emissions (B1) to high emissions (A1FI), with a range of scenarios in between.

For the IPCC Fifth Assessment Report (Stocker et al. 2013), scenario development focused on radiative forcing in the atmosphere. Here the emphasis was on adding different amounts of energy to the climate system over time. Scientists reviewed current estimates on radiative forcing, the total amount of extra energy entering the climate system throughout the 21st century and beyond. They used this information to construct a set of scenarios that would bound these estimates, from lesser amounts of energy entering the climate system to greater amounts of energy. These

Table 3.1—Scenarios used by climate models in the Special Report on Emission Scenarios (SRES) and representative concentration pathway (RCP) scenarios in the Intergovernmental Panel on Climate Change (IPCC) assessment reports.

	SRES scenarios	RCP scenarios
Definition	A plausible representation of the future development of emissions of substances that are potentially radiatively active (e.g., greenhouse gases, aerosols) based on a coherent and internally consistent set of assumptions about driving forces (such as demographic and socioeconomic development, technological change) and their key relationships. Concentration scenarios, derived from emissions scenarios, are used as input to a climate model to compute climate projections.	Scenarios that include time series of emissions and concentrations of the full suite of greenhouse gases and aerosols and chemically active gases, as well as land use/land cover (Moss et al. 2008). The word "representative" signifies that each RCP provides only one of many possible scenarios that would lead to the specific radiative forcing characteristics. The term "pathway" emphasizes that not only the long-term concentration levels, but also the trajectory taken over time to reach that outcome, are of interest (Moss et al. 2010).
Different scenarios	Scenario family is a set of scenarios that have a similar demographic, societal, economic, and technical change storyline. Four scenario families compose the SRES scenario set: A1, A2, B1, and B2.	RCP 2.6: One pathway where radiative forcing peaks at approximately 3 W m^{-2} before 2100 and then declines. RCP 4.5 and RCP 6.0: Two intermediate stabilization pathways in which radiative forcing is stabilized at approximately 4.5 W m^{-2} and 6.0 W m^{-2} after 2100. RCP 8.5: One high pathway for which radiative forcing reaches greater than 8.5 W m^{-2} by 2100 and continues to rise for some amount of time.
Use in models	Used to drive climate models in CMIP3[a]	Used to drive climate models in CMIP5.
Use in IPCC assessments	Houghton et al. (2001), Solomon et al. (2007).	Stocker et al. (2013).

[a] CMIP = Coupled Model Intercomparison Project; versions 3 and 5 are cited here.

scenarios are called representative concentration pathways (RCPs) (van Vuuren et al. 2011) because these scenarios represent one of many possible ways in which population, economic growth, and energy policy would lead to the specific radiative forcing characteristics. Consequently, the scenarios are defined by the amount of energy that is added to the atmosphere. For example, RCP 2.6 assumes a total radiative forcing increase of 2.6 Watts per square meter (0.82 British thermal units per square foot) by 2100, whereas RCP 8.5 assumes a much larger increase in the radiative forcing (8.5 Watts per square meter [2.7 British thermal units per square foot]). Intermediate scenarios include RCP 4.5 and RCP 6.0.

The RCPs focused on the implications of energy added to the atmosphere and consequently were not designed to mimic particular SRES scenarios. But because the SRES scenarios have been used for many analyses of climate change effects on natural resources (Walsh et al. 2014), an understanding of how the RCP and the SRES scenarios compare is helpful in interpreting past analyses. The comparison by Rogelj et al. (2012) considers climate sensitivity uncertainty, synthesizes the understanding of climate system and carbon cycle behavior, and is constrained by observed historical warming. Rogelj et al. (2012) identify analogs between RCP 4.5 and SRES B1, RCP 6.0 and SRES B2, and RCP 8.5 and SRES A1FI (table 3.2). The SRES A1B has a greater range in temperature changes than RCP 6.0, and a warmer upper range. Rogelj et al. (2012) note that temporal patterns differ between the SRES and RCP scenarios.

Climate Projections for the Region

This report uses scenarios RCP 4.5 and RCP 8.5 to explore future climate in the IAP region. These scenarios capture a moderate and a high future warming. In addition, more GCMs have used these scenarios than RCP 2.6 or RCP 6.0. The breadth of these scenarios and the availability of a larger set of projections enhance our understanding of the possible ranges in future climate. The term "climate projection" is used to describe the results of a climate model when forced by a particular scenario.

For an overview of projected future climate in the IAP region, we use the most recent climate change projections based on RCP 4.5 and RCP 8.5 scenarios (Stocker et al. 2013). Output from GCMs is at a scale too coarse to represent climate patterns in subregions and management areas relevant for the IAP. Therefore, we drew on climate projections that had been downscaled using the bias-correction and spatial disaggregation (BCSD) method (Maurer et al. 2007). We used projections from 36 climate models for RCP 4.5 and 34 climate models for RCP 8.5 (see Appendix 2). The variables available for each BCSD climate projection include monthly precipitation and monthly surface air temperature for the 1950–2099 period. Spatial resolution of the data is 1/8 degree latitude-longitude (about 7 square miles), and data cover the entire IAP region. Climate projections were archived by CMIP; hereafter climate projections that used SRES scenarios are referred to as "CMIP3" and climate projections that used the RCP scenarios as "CMIP5."

Historical mean annual temperature and precipitation vary across the IAP region (figs. 3.1, 3.2). We use a base period of 1979–2009 for the mean historical climate, and show mean temperatures and precipitation projected for two periods: 2030–2059 and 2070–2099. These time periods were selected to summarize climate that has influenced the current environmental conditions (base period) and two future periods that will be relevant to long-term management action (e.g., road construction, management of hydrological infrastructure, or vegetation planting). Historical mean

Table 3.2—Probabilistic estimates of temperature increase above preindustrial levels based on representative equilibrium climate sensitivity distribution for six Special Report on Emission Scenarios (SRES) market scenarios and four representative concentration pathway (RCP) scenarios (Rogelj et al. 2012).

	2090–2099		2100	
Scenario	Median	66% range	Median	66% range
	----- °F -----			
SRES B1	4.3	3.6–5.6	4.5	3.6–5.8
SRES A1T	5.2	4.5–6.7	5.4	4.5–6.8
SRES B2	5.2	4.3–6.3	5.4	4.7–6.7
SRES A1B	6.1	5.0–7.6	6.3	5.2–7.9
SRES A2	7.0	5.8–8.6	7.6	6.3–9.4
SRES A1F1	8.5	7.0–10.4	9.0	7.4–11.2
RCP 3-PD (2.6)	2.7	2.3–3.4	2.7	2.3–3.4
RCP 4.5	4.3	3.6–5.2	4.3	3.6–5.4
RCP 6.0	5.2	4.5–6.5	5.4	4.7–6.7
RCP 8.5	8.3	6.8–10.3	8.8	7.2–11.0

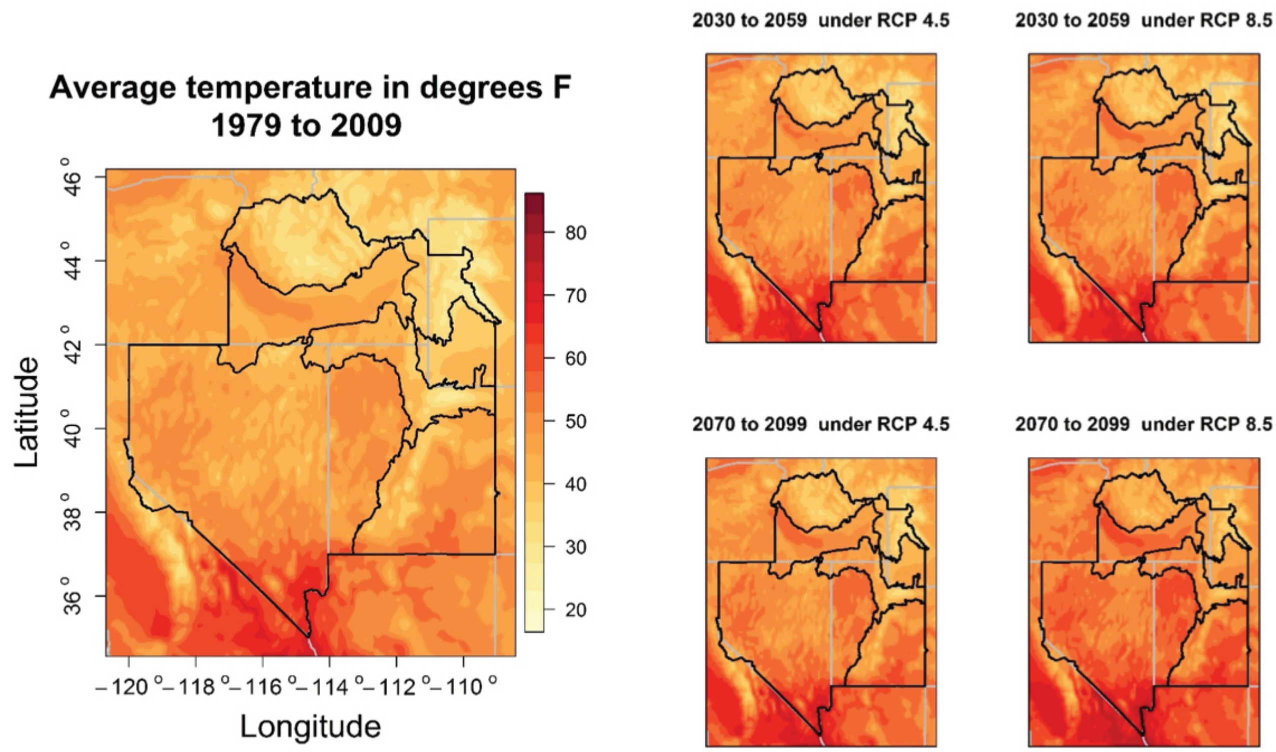

Figure 3.1—(a) Historical (1979–2009) and (b–e) projected (2030–2059 and 2070–2099) mean annual monthly temperature (°F) under RCP 4.5 and RCP 8.5 scenarios for the entire Intermountain Adaptation Partnership region. Projected climate is the 36-model mean for RCP 4.5 and the 34-model mean for RCP 8.5. Spatial resolution of the data is 1/8th degree latitude-longitude.

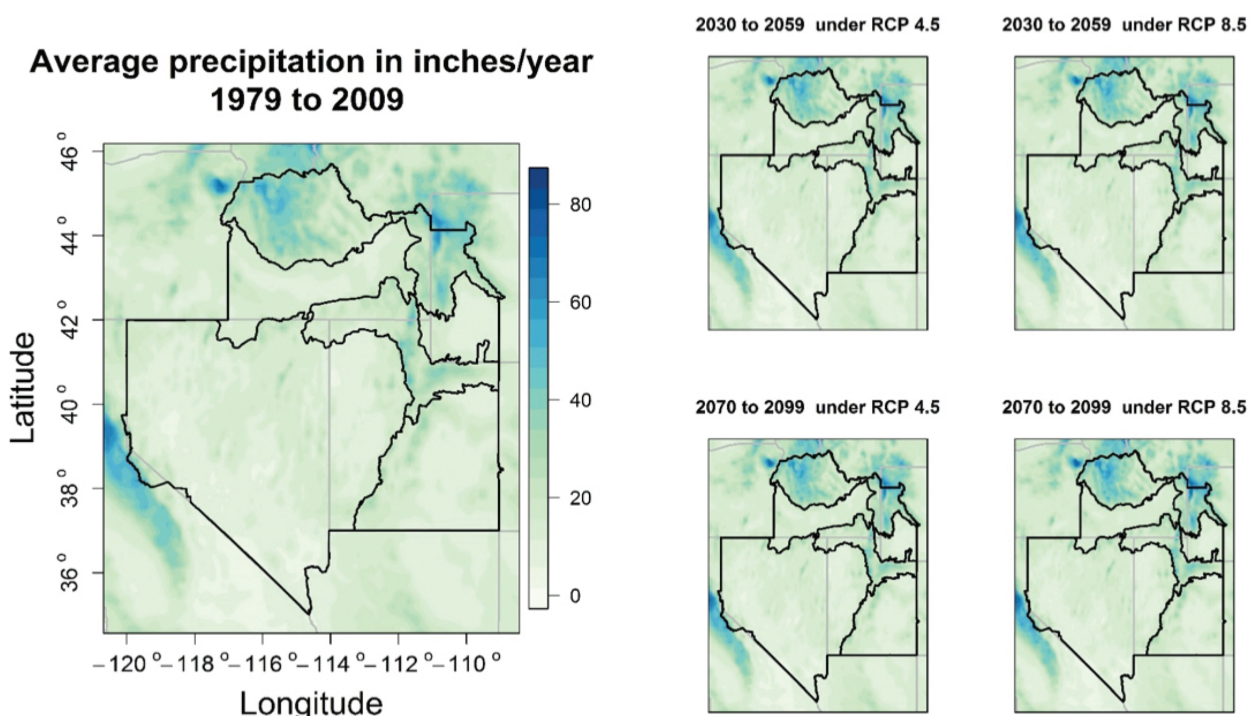

Figure 3.2—(a) Historical (1979–2009) and (b–e) projected (2030–2059 and 2070–2099) total annual precipitation (inches) under RCP 4.5 and RCP 8.5 scenarios for the entire Intermountain Adaptation Partnership region. Projected climate is the 36-model mean for RCP 4.5 and the 34-model mean for RCP 8.5. Spatial resolution of the data is 1/8th degree latitude-longitude.

annual temperatures can vary from nearly 20 °F to 75 °F within the IAP region. Historical total annual precipitation ranges from less than 3 inches to above 70 inches. All subregions of the IAP are expected to see increases in mean annual temperature. Temperatures are projected to increase more by the end-of-century period (2070–2099) and under the warmer scenario, RCP 8.5. Precipitation changes are less consistent; the northern parts of the IAP region may have precipitation increases.

Several resource chapters in this report have drawn on published literature about the effects of climate change on natural resources which used SRES scenarios and CMIP3 models. The question arises as to the regional differences between the CMIP3 projections under SRES scenarios and the CMIP5 projections under RCP scenarios. Understanding these differences may be helpful in interpreting the different projections used across these studies. Here, we compare CMIP5 climate projections under RCP 4.5 and RCP 8.5 scenarios from this study with CMIP3 models under the SRES scenario A1B, which has been used in several natural resource assessments, including the cold-water fisheries analysis in chapter 5.

To identify differences between these two sets of scenarios, we compare the projected changes in mean temperature with change in total annual precipitation over a common period for the IAP region. We obtained 10 CMIP3 global climate projections for the A1B scenario (moderate emissions) from Littell's group. We estimate the change in temperature and percentage change in precipitation between the future period (2040–2060) and the historical period (1979–2009) for the CMIP3 models that Littell et al. (2011) used and the CMIP5 models used in this study. In figure 3.3, the projected change in mean annual temperature is shown on the horizontal axis, and the percentage change in precipitation is shown on the vertical axis. Change is described as the difference in temperature and percentage change in precipitation between historical and projected future values. We show all CMIP5 models used in this study. We show only the mean (ensemble) of all 10 CMIP3 models and two individual models (pcm1 and miroc_3.2), as these projections from Littell et al. (2011) are used most often.

Across all CMIP5 models, projected change in temperature by the 2040–2060 period ranges from just under 2 °F to nearly 8 °F (fig. 3.3). Generally, the projected change for CMIP5 models under the RCP 8.5 scenario (shown in red) is greater than the change projected under the RCP 4.5 scenario (shown in yellow), but not always. For example, the RCP 8.5 projections for models FIO-ESM (number 15 in fig. 3.3) and MRI-CGCM3 (number 34 in fig. 3.3) show temperature changes that are less than the median changes for all RCP 4.5 models. The projected change in precipitation ranges from a decrease of about 12 percent to an increase of nearly 30 percent. However, 28 of the 36 projections under RCP 4.5 and 29 of the 34 projections under RCP 8.5 indicate an increase in precipitation. Across the IAP region, mean temperatures are projected to warm by 3.5 °F to almost

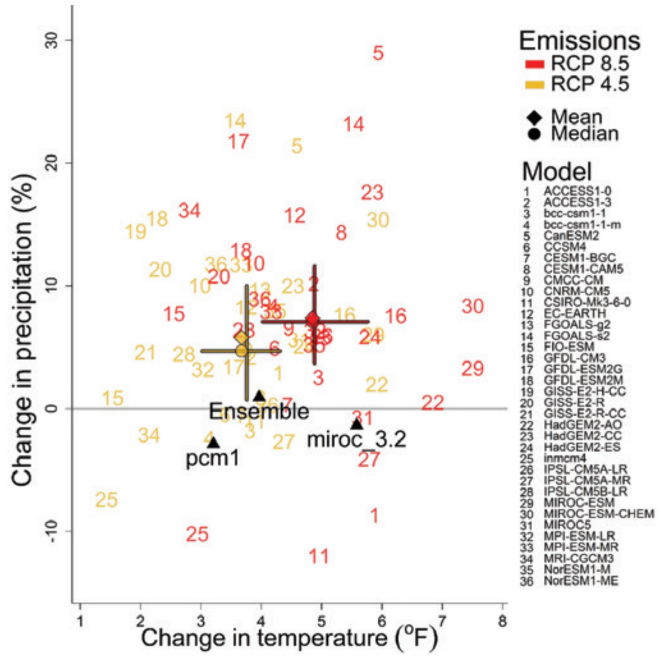

Figure 3.3—For the entire Intermountain Adaptation Partnership region, change in mean annual temperature (°F) and total annual precipitation (%) from the simulated historical climate (1979–2009) and the projected climate (2040–2060) using the CMIP5 RCP 4.5 and RCP 8.5 scenarios and the CMIP3 A1B scenario. Each CMIP5 model result is labeled by a number with a key in the legend (e.g., 29 is MIROC-ESM) in colors to indicate RCP 4.5 (yellow) and RCP 8.5 (red) (see table 3.2). The crosses in the middle represent the median and 25 to 75 percent of the RCP 4.5 and the RCP 8.5 projections used in this study. The mean values for the CMIP5 changes are shown on the figure as colored diamonds. The CMIP3 results are labeled in black triangles (see table 3.2 and Littell et al. [2011]).

5 °F over the next 50 years, with precipitation projected to increase slightly, by 5 to 8 percent.

The CMIP3 projections for the A1B scenario are within the mean temperature range of the CMIP5 projections (fig. 3.3). The A1B ensemble projection of a nearly 4 °F increase in temperature is similar to the mean increase for the RCP 4.5 scenario; both of these scenarios are considered moderate in terms of future warming. The two individual model projections under the A1B scenario span the temperature range of the individual model projections under RCP 4.5. For precipitation, the CMIP3 models under the A1B scenario project a slight increase (ensemble) and decreases in precipitation (pcm1 and miroc_3.2). We conclude that when this set of CMIP3 results are compared with CMIP5 results for the IAP region, future temperatures are projected to be similar. However, CMIP5 precipitation projections collectively show a greater likelihood of increases in precipitation than the CMIP3 projections (fig. 3.3). This slight increase in projected precipitation with the CMIP5 models might be considered when evaluating the impact of analyses using CMIP3 climate projections.

Climatic Variability and Change in the Subregions

Historical Climate

To understand historical climatic variability and trends at the subregional scale in the IAP region, we compared three gridded datasets: Parameter-elevation Regressions on Independent Slopes Model (PRISM) (PRISM Climate Group 2014), Maurer (Maurer et al. 2002), and TopoWx (Oyler et al. 2015a). These three datasets used observed point measurements of precipitation, temperature, and other climatic factors to produce continuous, digital grid estimates of monthly, yearly, and event-based climatic parameters. Because of differences in the station data used by these gridded products as well as the models and assumptions used to interpolate to a grid, these models do not always agree on the historical climate or trend for a region. For example, in the western mountains, PRISM has been shown to have an artificial amplification in warming trend (Oyler et al. 2015b).

The Middle Rockies subregion encompasses central Idaho, an area known as the "Idaho Batholith," and the Salmon River Mountains. Climate is strongly influenced by interactions with topography, elevation, and aspect. Westerly winds bring in moisture from the Pacific Ocean, but moisture is precipitated over the western blocking mountains. Elevations range from 3,000 to 10,000 feet, with the highest peaks in the Salmon River Mountains. The deep dissections of this subregion can be seen in the ridge patterns in temperature (fig. 3.1a) and large gradients in precipitation (fig. 3.2a).

Climate in the Middle Rockies is characterized by cold winters with moderate to heavy snow accumulations at higher elevations. Throughout the 1940–2009 period, mean minimum temperatures showed a distinct increasing trend (fig. 3.4). Mean maximum temperature ranged from 48 to 54 °F over this period (fig. 3.5). As with other subregions, no warming trend is evident across the entire time period. In the last 25 years, however, the Middle Rockies maximum temperatures showed a slight increasing trend (fig. 3.5); similar increasing trends in summer temperatures were noted by Isaak et al. (2010) for the Upper Boise River watershed. Annual precipitation over the historical period ranged from 20 inches to greater than 35 inches per year. Precipitation patterns were highly variable, with a slight downward trend in the last 25 years (fig. 3.6).

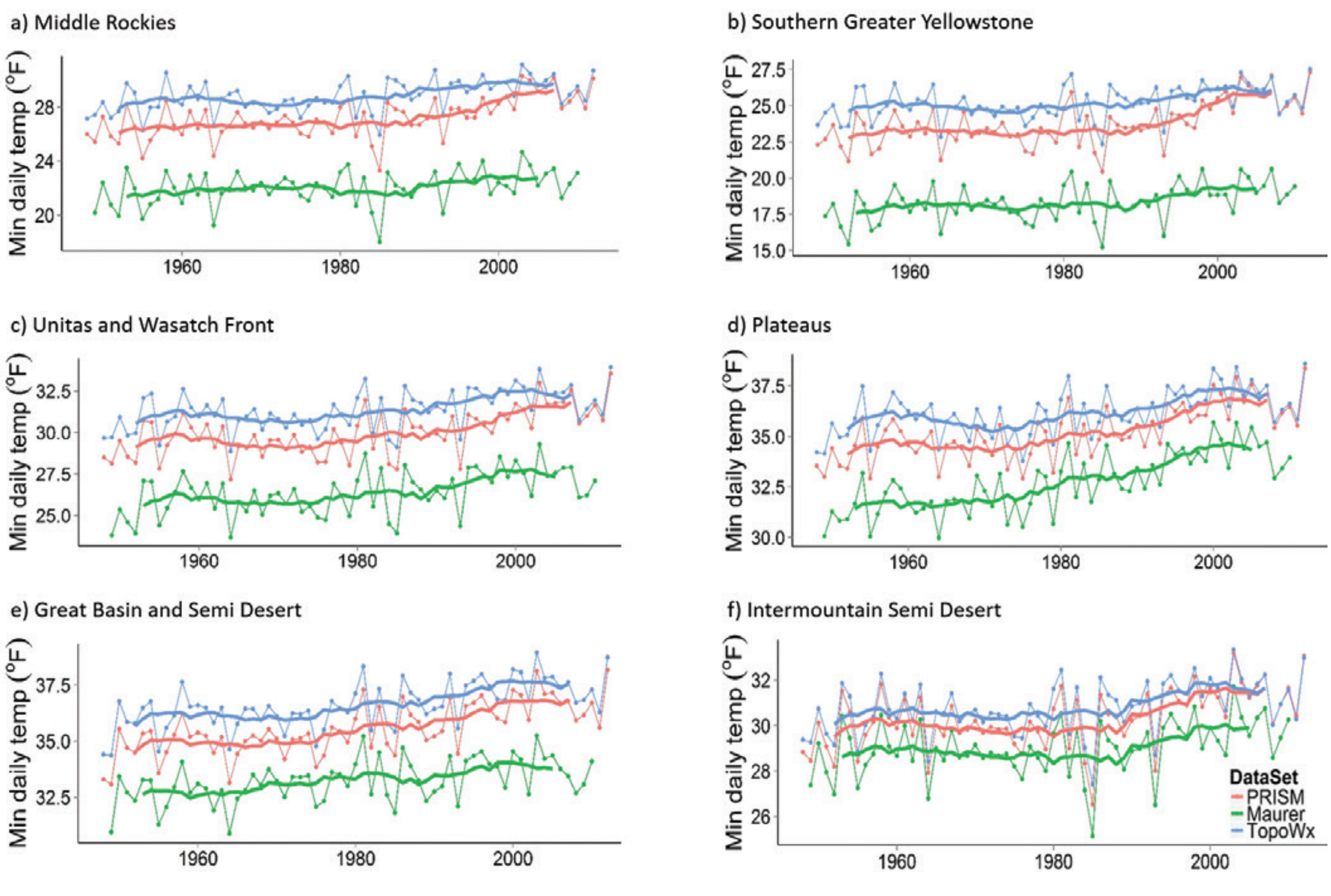

Figure 3.4—Annual historical mean monthly minimum temperature from the monthly gridded PRISM, Maurer, and TopoWx datasets for 1949–2010 for all six subregions of the Intermountain Adaptation Partnership region. The heavy lines are the 10-year rolling average from each dataset to show short-term trends.

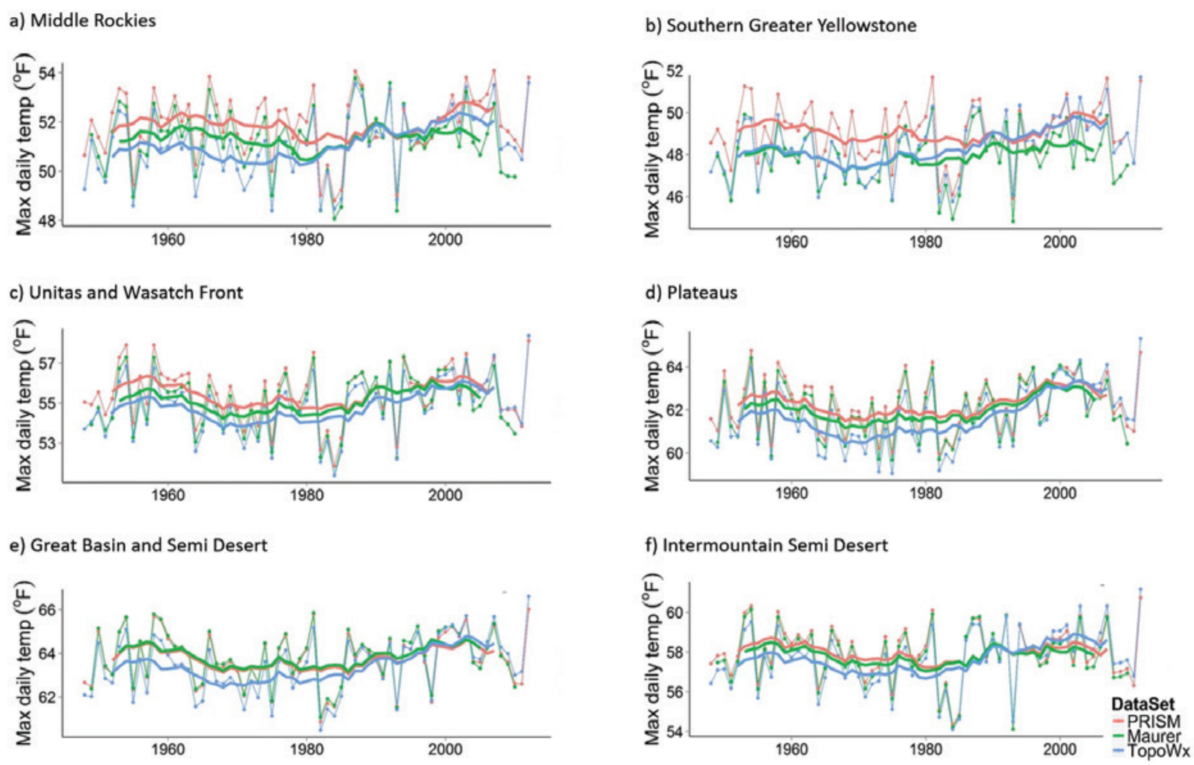

Figure 3.5—Annual historical mean monthly maximum temperature from the monthly gridded PRISM, Maurer, and TopoWx datasets for 1949–2010 for all six subregions of the Intermountain Adaptation Partnership region. The heavy lines are the 10-year rolling average from each dataset to show short-term trends.

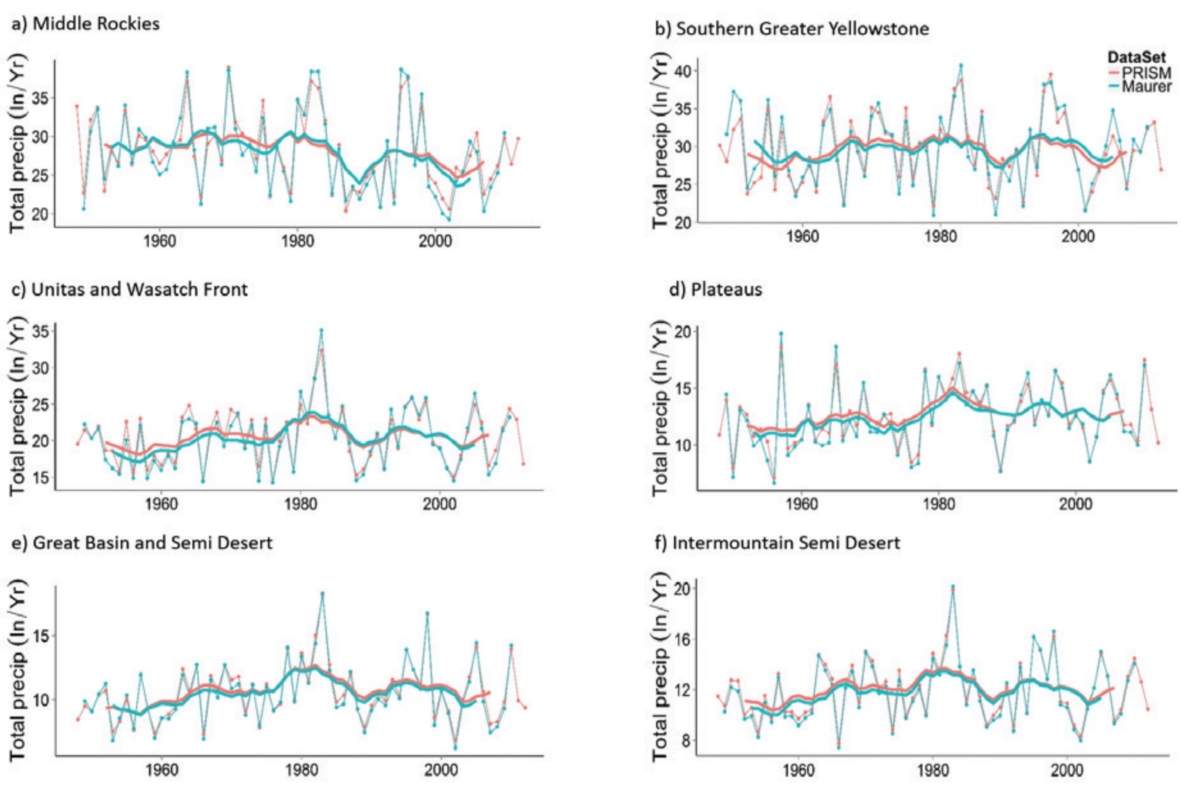

Figure 3.6—Historical total annual precipitation from the monthly gridded PRISM and Maurer et al. (2007) datasets for 1949–2010 for all six subregions of the Intermountain Adaptation Partnership region. The heavy lines are the 10-year rolling average from each dataset to show short-term trends.

The Southern Greater Yellowstone subregion includes Grand Teton National Park, and the Targhee and Bridger-Teton National Forests. This subregion and the Middle Rockies are the coldest subregions (figs. 3.4, 3.5). Mean minimum temperatures in the Southern Greater Yellowstone subregion showed an increasing trend over the last 50 years of the historical period (fig. 3.4). Monahan and Fisichelli (2014) reported that recent annual mean temperatures (last 10-, 20-, or 30-year periods) for Grand Teton National Park were higher than 90 percent of the historical temperatures over the 1901–2012 period. They also found that recent minimum temperatures in the coldest month (last 10-, 20-, or 30-year periods) were greater than 95 percent of the historical record. In contrast, maximum temperatures showed an increasing trend only during the last 25 years (fig. 3.5).

Climate in the Southern Greater Yellowstone subregion, as in the Middle Rockies, is strongly influenced by the mountains and interactions among topography, elevation, and aspect. Few mountains block the western passage of moist air from the Pacific Ocean to the Teton Range; consequently, the Teton Range, along with portions of southwestern Yellowstone National Park, are among the wettest areas in the larger Greater Yellowstone Area. Annual precipitation on the west side of the Teton Range can exceed 70 inches, with most of this precipitation falling as snow. In contrast, precipitation on the east side of the Teton Range can be as little as 19 inches (Davey et al. 2006). The Southern Greater Yellowstone subregion is the wettest in the IAP region (fig. 3.6). No trend is found in annual precipitation over the last 50 years although distinct wet and dry periods occurred. Davey et al. (2006) describe a 6-year drought (1999–2005) as the longest drought in the Grand Teton National Park since the Dust Bowl drought of the 1930s.

Climate in the Uintas and Wasatch Front can be characterized as humid continental, with warm to hot summers, cold winters with abundant snowfall, and no distinct dry period (Gillies and Ramsey 2009). As with the Middle Rockies and the Southern Greater Yellowstone subregions, climate in this subregion is strongly influenced by the terrain and interactions among topography, elevation, and aspect. The Wasatch Range generally runs north to south, and the Uinta Mountains extend east and west. These ranges crest above 10,000 feet, with the highest point of 13,498 feet at Kings Peak in the Uinta Mountains. As in most of the subregions, minimum temperatures trended upward over the last 50 years (fig. 3.4). Mean maximum temperatures were between about 53 and 57 ^{o}F, with no clear trends over the historical period (fig. 3.5). Gillies et al. (2012) concluded that during the last half-century, the proportion of winter (January–March) precipitation falling as snow across Utah has decreased by 9 percent, the result of a significant increase in rainfall combined with a minor decrease in snowfall. Although warming temperatures play a role, climate features such as circulation patterns also contribute to these changes.

Mean annual precipitation within the Uintas and Wasatch Front subregion ranged from 10 inches to more than 40 inches (fig. 3.6). Over the last 50 years, precipitation exhibited no annual trend, although dry or wet periods are evident. Morrisette (1988) reported that the 1982–1986 precipitation reached 134 percent of normal in the Salt Lake drainage area, resulting in historically high levels in the Great Salt Lake. Using tree-ring analyses, DeRose et al. (2015) concluded that 1986 was the fourth wettest year over the last 1,200 years in the Bear River watershed. They also reported that although the later part of the 20th century was the second wettest period (40 years), the first half was the fourth driest period in the past 1,200 years. Using tree rings to reconstruct streamflow for the Weber River, Bekker et al. (2014) reported that the 20th-century instrumental record includes the fewest extreme dry years in the 576-year, tree-ring-based reconstruction. In the Uinta Mountains, severe droughts have occurred, on average, two to five times per century (MacDonald and Tingstad 2007). Strong decreases in winter precipitation characterized the major droughts in the Uinta Mountains: the 1930s Dust Bowl event, the 1976–1977 event, and the 1987–1989 event. These later two droughts were related to decreases in eastern Pacific Ocean sea surface temperatures (MacDonald and Tingstad 2007). Droughts in the Wasatch Range occurred during the 1400s and 1500s; even though droughts were fewer in the 1700s and 1800s, they had longer duration (Bekker et al. 2014). The tree-ring studies consistently emphasize the importance of local conditions in understanding climate-vegetation relationships (Louderback et al. 2015).

The Plateaus subregion encompasses three ecological provinces of the Colorado Plateau. The Uinta Basin is a gently rolling plateau that the Green River and its tributaries have eroded into many spectacular canyons (Leydsman McGinty and McGinty 2009). In the High Plateaus province, north-south trending faults and valleys separate individual plateaus, such as the Awapa, Aquarius, and Paunsaugunt Plateaus (Leydsman McGinty and McGinty 2009). The Uinta Basin and the High Plateaus are cooler than the Canyonlands province. The Colorado River has eroded the Canyonlands into many deep, sheer-walled canyons, plateaus, mesas, buttes, and badlands. In addition, the La Sal and Abajo Mountains rise above the Colorado Plateau in southeastern Utah. Precipitation in this subregion ranges from 14 to 35 inches, with the highest precipitation in the High Plateaus province.

Minimum temperatures in the Plateaus subregion showed an upward trend over the entire historical period (fig. 3.4). Mean maximum temperature in the subregion ranged between 59 and 65 ^{o}F over the last 50 years, showing a slight upward trend after 1980 (fig. 3.5). No trend is seen in precipitation over the last 50 years, although higher precipitation occurred in the 1980s (fig. 3.6). Tree-ring reconstruction of precipitation from 1200–2001 in the Uinta Basin indicates significant precipitation variability at inter-annual to decadal scales, with more severe dry events prior to 1900 than after (Gray et al. 2004).

The Great Basin and Semi Desert subregion has great climatic diversity (Svejcar et al. 2016). The surrounding mountains, as well as the mountains within, strongly influence the climate of this subregion. A series of north-south mountain ranges within the subregion are interspersed among low-elevation basins, resulting in wide local variations in temperature and precipitation (fig. 3.1). Elevation ranges from less than 1,500 feet to more than 10,000 feet. Extreme temperatures can range from -15 to 120 °F (WRCC 2016b,c).

The Great Basin and Semi Desert subregion is the warmest of the subregions. For the larger Southwest region in the United States, Kunkel et al. (2013) reported an increase in mean annual temperature, with greater warming for minimum temperature than maximum temperature, over the last 115 years. That pattern for minimum and maximum monthly temperature was also seen in this subregion; mean minimum temperatures ranged from 30 to 38 °F (fig. 3.4) and mean maximum temperatures from 60 to 66 °F (fig. 3.5).

The primary source of moisture for the Great Basin and Semi Desert subregion is the Pacific Ocean, with seasonal monsoonal influences from the Gulf of Mexico. Much of the moisture from the Pacific Ocean is lost through orographic precipitation as the moisture flows upward and then over the bordering Sierra Nevada and Cascade Range. Mean annual precipitation varied from less than 8 inches to more than 15 inches over the last 50 years (fig. 3.6), with wet and dry years evident. Annual snowfall ranges from less than 1 inch to 124 inches (WRCC 2016b,c).

The Intermountain Semi Desert subregion includes two distinct areas: the large valley encompassing the Snake River plains in Idaho, and the southwestern area in Wyoming (Chapter 2). The long, large valley in Idaho gradually rises in elevation from 3,300 feet in the Magic Valley, through the Lower Snake River Plain, to the eastern end of the Upper Snake River Plain at 5,600 feet (Andretta and Geerts 2010). Swan Falls, on the Snake River in Idaho, has a mean annual temperature of 55 °F (WRCC 2016a). The Central Mountains, where the Boise, Payette, Salmon-Challis, and Sawtooth National Forests are located, bound this valley to the north. To the south and east of this subregion lies the Southern Highlands at elevations from 6,500 to 8,200 feet, Eastern Highlands, and Upper Snake Highlands of Idaho. As with the Great Basin and Semi Desert subregion, topography plays a role in the climate; however, with fewer barriers to the west, this area of the subregion receives greater moisture (fig. 3.2).

The Wyoming portion of this subregion encompasses the Green River Basin, a valley bounded on the northern edges by the Gros Ventre Mountains to the west and the Wind River Mountains to the east. The nearly 4,000-square-mile area is high, dry sagebrush-steppe, basically a desert where winter brings wind and cold, and little snow (Ostlind 2011). Temperatures are cooler in the Wyoming section than in the Idaho valley (fig. 3.1); mean annual temperature for Big Piney in the northern part of Green River Basin is 36 °F, making for a short growing season. Winter extremes can reach -50 °F as cold air settles in the Green River Basin.

Mean minimum temperatures for this subregion showed a slight warming trend over the 1949–2010 period (fig. 3.4). Mean maximum temperatures during this time ranged from about 55 to 60 °F, with little trend (fig. 3.5). Hoekema and Sridhar (2011) reported regional warming in the Snake River Basin, particularly in spring, over the last 35 years. This subregion and the Great Basin and Semi Desert are the driest subregions. Annual precipitation in the Intermountain Semi Desert subregion is generally between 8 and 12 inches (fig. 3.6). Precipitation showed no trend over the historical period.

Projected Climate

Changes in annual and seasonal temperature and precipitation are summarized by subregion in table 3.3. Trends in annual and seasonal temperature and precipitation projections are shown as figures for each subregion (see box 3.1 for more information on the format of these subregional figures): Middle Rockies (figs. 3.7–3.9), Southern Greater Yellowstone (figs. 3.10–3.12), Uintas and Wasatch Front (figs. 3.13–3.15), Plateaus (figs. 3.16–3.18), Great Basin and Semi Desert (figs. 3.19–3.21), and Intermountain Semi Desert (figs. 3.22–3.24).

In the future, all subregions in the IAP are projected to see increases in annual and seasonal minimum and maximum temperatures, with greater changes under the RCP 8.5 scenario by 2100 than under the RCP 4.5 scenario (table 3.3). Within each subregion, temperatures vary greatly across landscapes, the result of topography and aspect. In the Middle Rockies, the projected increase in minimum temperature under the RCP 8.5 scenario will bring the subregional median temperature above freezing (fig. 3.7a); this projected increase suggests that for some areas in the IAP region, a biologically meaningful threshold could be crossed. Similar patterns for an increase in median minimum temperature above freezing occur in the Southern Greater Yellowstone subregion under the RCP 8.5 scenario only (fig. 3.10), and Uintas and Wasatch Front (fig. 3.13), the Plateaus (fig. 3.16), and the Intermountain Semi Desert subregions (fig. 3.22) under both scenarios. For most subregions, annual precipitation projections are highly variable with no discernible trend over time or between the two scenarios. However, slight increases in annual precipitation are projected under the RCP 8.5 scenario for the Middle Rockies, the Southern Greater Yellowstone, and the Intermountain Semi Desert subregions (figs. 3.7, 3.10, 3.22), which lie in the northern part of the IAP region.

Seasonal temperatures across the subregions are projected to increase and may cross biologically meaningful thresholds in particular seasons (table 3.3). Minimum seasonal temperatures are projected to rise in all seasons across all subregions under both the RCP 4.5 and RCP 8.5 scenarios (figs. 3.8, 3.11, 3.14, 3.17, 3.20, 3.23). Maximum seasonal temperatures are also projected to rise in all seasons under both RCP 4.5 and RCP 8.5 across all

Table 3.3—Summary of projected changes in annual and seasonal temperature, and precipitation for each Intermountain Adaptation Partnership subregion.

Subregion	Temperature	Precipitation	Seasonality
Middle Rockies	By 2100, median maximum temperature is projected to rise about 6 °F under RCP 4.5 and about 10 °F under RCP 8.5; the two ensemble projections begin to diverge after 2045. Median minimum temperature is projected to rise about 5 °F under RCP 4.5 and about 10 °F under RCP 8.5.	Annual precipitation projections are highly variable with no discernible trend under RCP 4.5 and a slight increasing trend under RCP 8.5.	Maximum temperatures are projected to increase by 5 to 10 °F across the seasons. The greatest departure from historical seasonal minimum temperatures occurs in summer. Over the historical period, summer minimum temperatures ranged around the mid- to upper 30s. By 2040, the projected median is 40 °F and rises to nearly 50 °F under the RCP 8.5 scenario by 2100 (fig. 3.9). By 2100, the median projections for spring, summer, and fall under the RCP 8.5 scenario are outside of historical ranges.
Southern Greater Yellowstone	By 2100, median maximum temperature is projected to rise about 5 °F under RCP 4.5 and about 11 °F under RCP 8.5; projections for the two RCPs begin to diverge around 2040. By 2100, median minimum temperature is projected to increase about 6 °F under RCP 4.5 and about 12 °F under RCP 8.5. Median minimum temperatures are projected to remain below freezing under RCP 4.5. However, minimum temperatures are likely to rise to just under freezing by 2100 under RCP 8.5.	Annual precipitation projections are highly variable with no discernible trend under RCP 4.5 and a slight increasing trend under RCP 8.5.	Maximum temperature is projected to increase in all seasons, with winter temperatures rising about 3 °F and all other seasons rising about 5 °F under RCP 4.5 by the end of the 21st century. Under the warmest scenario, seasonal temperatures increase about 10 °F in winter, spring, and fall, but by more than 12 °F in summer by the end of the 21st century. Median minimum temperatures for all seasons by the 2080s are projected to be outside of historical ranges in the warmest scenario. Median minimum spring and fall temperatures are projected to increase, such that some projections rise above freezing by the end of the 21st century under the RCP 8.5 scenario.
Uintas and Wasatch Front	By 2100, median maximum temperature is projected to rise about 5 °F under RCP 4.5 and about 11 °F under RCP 8.5. Projections for the two scenarios begin to diverge around 2040. By 2100, median minimum temperature is projected to rise about 5 °F under RCP 4.5 and about 12 °F under RCP 8.5. Median minimum temperatures are projected to rise above freezing in both scenarios (by 2050 under RCP 8.5 and by 2075 under RCP 4.5).	Annual precipitation projections are highly variable with no discernible trends.	Maximum temperatures are projected to increase in all seasons, with winter temperatures rising about 4 °F and all other seasons rising about 6 °F under RCP 4.5 by the end of the 21st century. Maximum median temperatures by the 2080s are outside of the historical range of values for all seasons in the warmest scenario. Median minimum spring and fall temperatures are projected to rise above freezing by the 2080s in both scenarios. The greatest departure from historical seasonal minimum temperatures occurs in summer.

Table 3.3—*Continued.*

Subregion	Temperature	Precipitation	Seasonality
Plateaus	By 2100, median maximum temperature is projected to rise about 5 °F under RCP 4.5 and about 10 °F under RCP 8.5. By 2100, median minimum temperature is projected to rise about 5 °F under RCP 4.5 and about 12 °F under RCP 8.5; the two ensemble projections begin to diverge after 2050. By 2050, median minimum temperature is projected to rise above freezing in both scenarios.	Precipitation projections are highly variable with no discernible trend over time or between the two scenarios.	Maximum temperature is projected to increase in all seasons by about 5 °F under RCP 4.5 and by about 10 °F under RCP 8.5 by the end of the 21st century. The greatest departure from historical temperatures by 2100 is projected to occur in summer, where median temperatures rise above 95 °F under the RCP 8.5 scenario. Projected median maximum temperatures for winter, spring and autumn are also outside of historical ranges by end of the 21st century. The greatest departure from historical seasonal minimum temperatures is projected to occur in summer. Minimum temperatures in summer are projected to rise about 6 °F by 2100 under RCP 4.5 and over 10 °F under RCP 8.5, with the variation well outside of the historical ranges.
Great Basin and Semi Desert	By 2100, median maximum temperature is projected to rise about 5 °F under the RCP 4.5 scenario and about 10 °F under the RCP 8.5 scenario. Historically median minimum temperature has ranged around freezing; in the near future, it is projected to rise above freezing, and by end of century, is projected to increase by 6 to 10 °F. The two ensemble projections begin to diverge after 2050.	Precipitation projections are highly variable with no discernible trend over time or between the two scenarios.	Maximum temperature is projected to increase by 5 °F in winter and spring under the RCP 4.5 scenario and by 10 °F under the RCP 8.5 scenario by the end of the 21st century. Summer and fall temperatures are projected to increase by 12 °F by the end of the 21st century under the RCP 8.5 scenario. Median minimum spring temperatures rise above freezing for both scenarios by 2100 and for the RCP 8.5 scenario, temperatures approach 40 °F. Median minimum and maximum projections for the both scenarios in all seasons by 2100 are outside of the historical range.
Intermountain Semi Desert	By the mid-21st century, median maximum temperature is projected to rise about 5 °F under RCP 4.5 and about 10 °F under the RCP 8.5. Median minimum temperature is projected to rise about 5 °F under RCP 4.5 and about 11 °F under RCP 8.5. By 2100, the projected changes for minimum temperature rise above freezing.	The highly variable precipitation projections show no discernible trend over time under the RCP 4.5 and suggest a slight increase under the RCP 8.5 scenario.	Maximum temperature increases in all seasons to the end of the 21st century in both climate scenarios. The greatest departure from historical temperatures by 2100 occurs in summer under RCP 8.5, when projected mean temperatures approach 95 °F, nearly 15 °F above historical temperature. Median minimum seasonal temperatures are projected to rise in all seasons. Median minimum and maximum values for all seasons under the RCP 8.5 scenario are outside of the historical ranges by 2100.

subregions (figs. 3.9, 3.12, 3.15, 3.18, 3.21, 3.24). Thus, the frequency of days with extreme heat in summer is likely to increase. Winter precipitation is an important reservoir for mountain and surrounding lower elevation communities. Few subregional or site-specific projections for snowpack have been made for the IAP region. For the Wasatch Range and Uinta Mountains, Klos et al. (2014) used only RCP 8.5 and 20 climate models (similar to the projections used in this chapter), and they report that these ranges will have fall-through-spring temperatures such that wintertime precipitation will begin to shift from strongly snow dominated to a mixed rain-snow regime by the mid-21st century. The shoulder months of November and March will shift to rain, with December through February retaining a snow-dominated system longer. For additional discussion of snowpack and climate change, see Chapter 4. Also see Rice et al. (2017) for a review of climate change literature for the Uintas and Wasatch Front area.

Box 3.1—Template for Projected Climate Change Figures

For each of the six subregions, a common template for figures has been used to describe the projected climate. The first figure for each subregion (figs. 3.7, 3.10, 3.13, 3.16, 3.19, 3.22) shows the historical simulations and projections for annual daily minimum and maximum mean temperatures (°F), and total annual precipitation (inches) under the RCP 4.5 and RCP 8.5 scenarios based on the CMIP5 BCSD data. These figures show the historical climate simulations by the CMIP5 models, which reflect the pre-2010 climate forcings. These historical simulations are bias corrected and downscaled in the same manner as model future projections. In these figures, we overlaid the gridded historical observation data (blue line) from Maurer et al. (2002). In most regions, the historical simulated minimum and maximum temperatures and annual precipitation are less variable than the historical observed gridded climate. The future projections are shown in colors: red for RCP 8.5 and yellow for RCP 4.5. The ensemble median from all 20 models for each scenario is shown in the heavy line; the 5th- and 95th-percent quantiles for all models are shown by the shaded area. Typically, climate projections under the higher emissions scenario (RCP 8.5) will indicate a higher temperature by 2100 than climate projections under the RCP 4.5 scenario.

The second figure for each subregion (figs. 3.8, 3.11, 3.14, 3.17, 3.20, 3.23) shows the seasonal daily minimum temperature (°F) for the historical and projected period 1950–2100. Winter is defined as the months of December, January, and February. Spring is defined as March, April, and May; summer as June, July, and August; and fall as September, October, and November. We use box plots here, where each box is an aggregation of 20 years of modeled historical or projected seasonal data. For example, the box labeled “1960” represents the seasonal average of 1950 to 1969. We used the 20-year period here to explore the temporal changes over this century. The modeled historical boxes are gray, and boxes for projections use the same colors as in other figures: yellow for RCP 4.5 and red for RCP 8.5. The central line in each box is the median, indicating the same number of modeled historical or projections above and below this line. The hinges or edges of the boxes are the first and third quartiles. Whiskers extend past the first and third quartile by 1.5 times the interquartile range.

The third figure for each subregion (figs. 3.9, 3.12 3.15, 3.18, 3.21, 3.24) shows the seasonal daily maximum temperature (°F) for the historical and projected period. These figures are set up in the same way as the second figures. There is large variability and no discernible trend in the seasonal precipitation projections, and hence, less confidence overall in the finer scale precipitation projections; these figures are not shown here.

Summary and Conclusions

For this overview, the projected climate was derived from climate models in the CMIP5 database, which was used in the most recent IPCC reports. We quantified changes in temperature and precipitation by the 2040 period (2030–2059) and 2080 period (2070–2099). Over the next 100 years, annual minimum and maximum temperatures are projected to rise by as much as 10 °F in the IAP region. Projections for annual precipitation are highly variable. For most subregions in the IAP area, precipitation remains variable; slight increases in total annual precipitation are projected for the Middle Rockies, Southern Greater Yellowstone, and Intermountain Semi Desert subregions under the RCP 8.5 scenario. As with annual temperature, winter, spring, summer, and fall temperatures are projected to increase, with summer temperatures showing the greatest increases in several subregions. For many subregions, the seasonal temperatures by end of century are outside of the historical observed ranges. Many of the resource chapters draw from existing scientific literature that used climate projections from the 2007 IPCC reports (the CMIP3 database). In mid-century (2040–2060), CMIP3 and CMIP5 temperature projections are similar. However, CMIP5 precipitation projections appear to be slightly wetter than those in CMIP3.

Acknowledgments

We acknowledge the World Climate Research Programme’s Working Group on Coupled Modelling, which is responsible for CMIP, and we thank the climate modeling groups (listed in Appendix 2) for producing and making available their model output. For CMIP, the U.S. Department of Energy’s Program for Climate Model Diagnosis and Intercomparison provides coordinating support and led development of software infrastructure in partnership with the Global Organization for Earth System Science Portals. Contributions from Marian Talbert were supported by the Department of the Interior’s North Central Climate Science Center. We appreciate the contributions of Jeff Morisette to the development of the chapter and the workshop presentations.

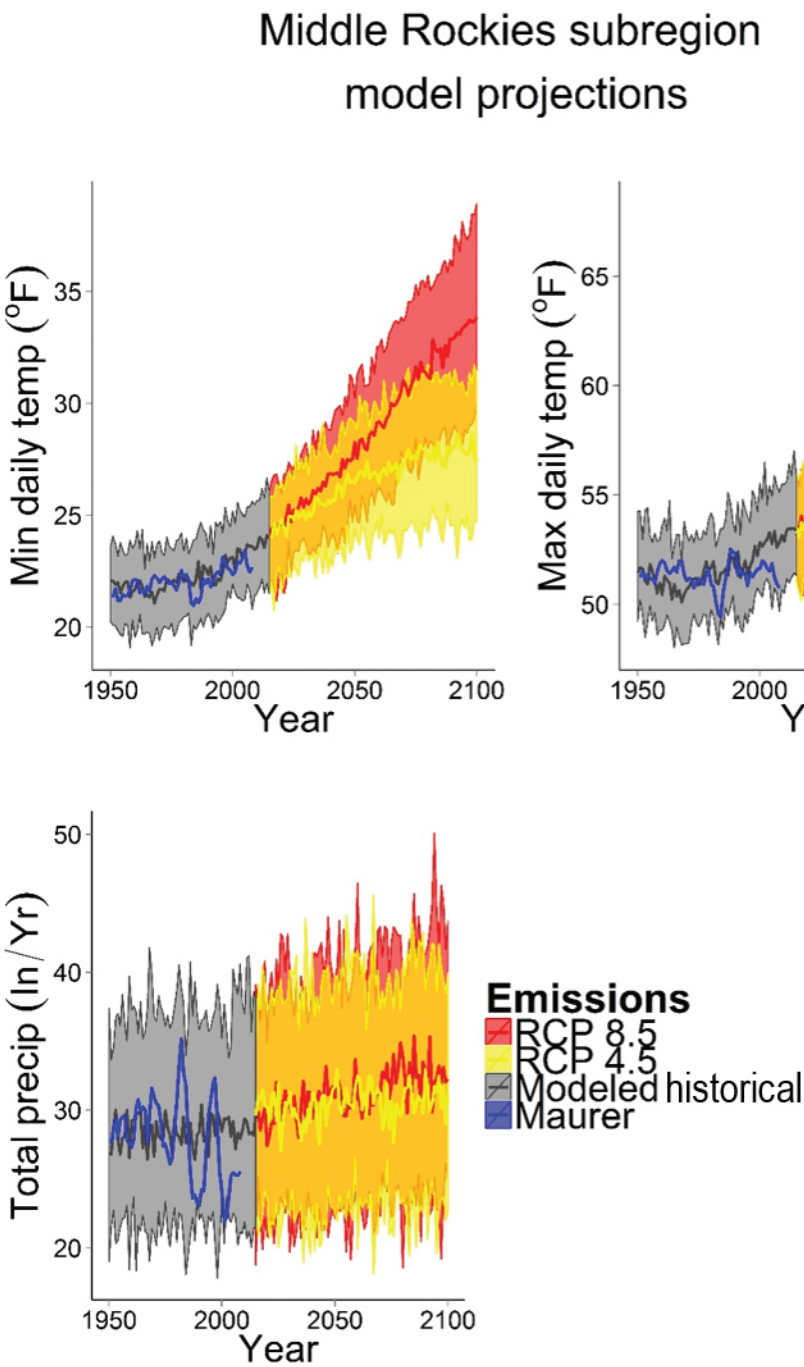

Figure 3.7—Historical modeled and projected annual mean monthly minimum temperature, annual mean monthly maximum temperature, and total annual precipitation for 1950–2100 under RCP 4.5 and RCP 8.5 emissions scenarios based on CMIP5 data for the Middle Rockies subregion of the Intermountain Adaptation Partnership region. Historical annual data from the gridded Maurer et al. (2007) dataset are also shown. See box 3.1 for further explanation.

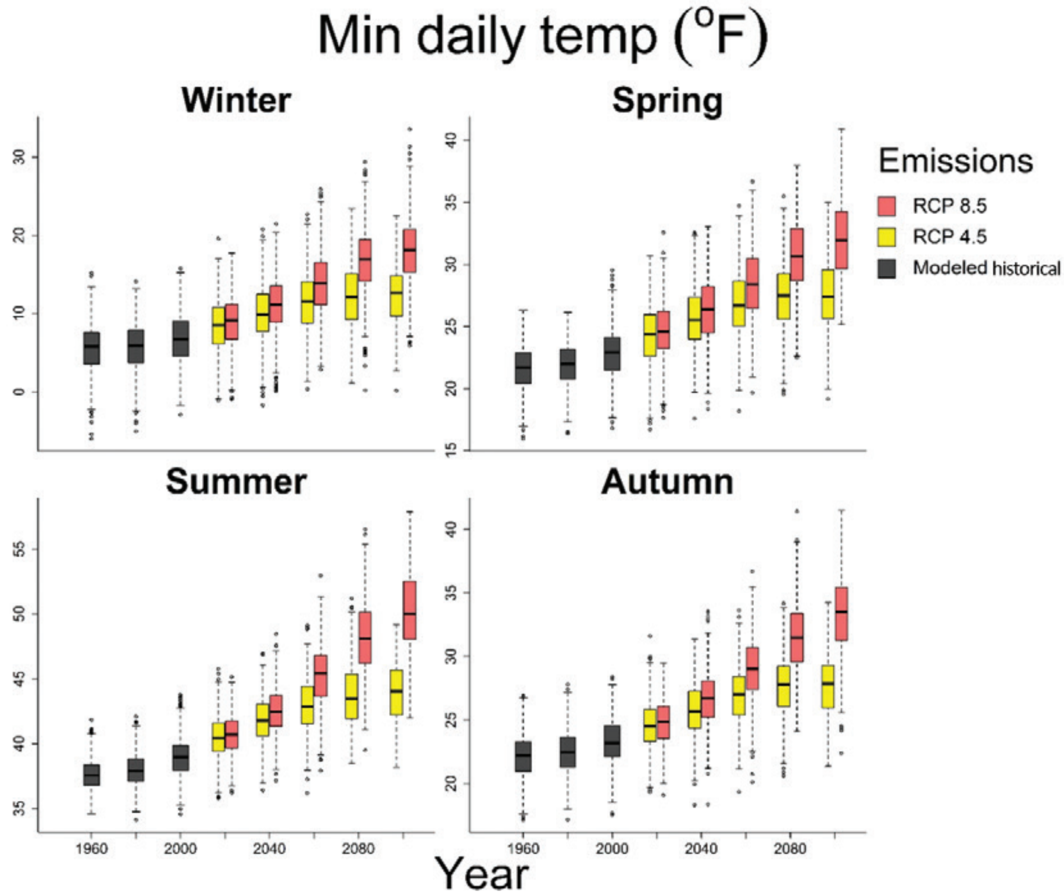

Figure 3.8—Historical modeled and projected seasonal mean monthly minimum temperature for 1950–2100 under RCP 4.5 and RCP 8.5 emissions scenarios for the Middle Rockies subregion of the Intermountain Adaptation Partnership region. See box 3.1 for further explanation.

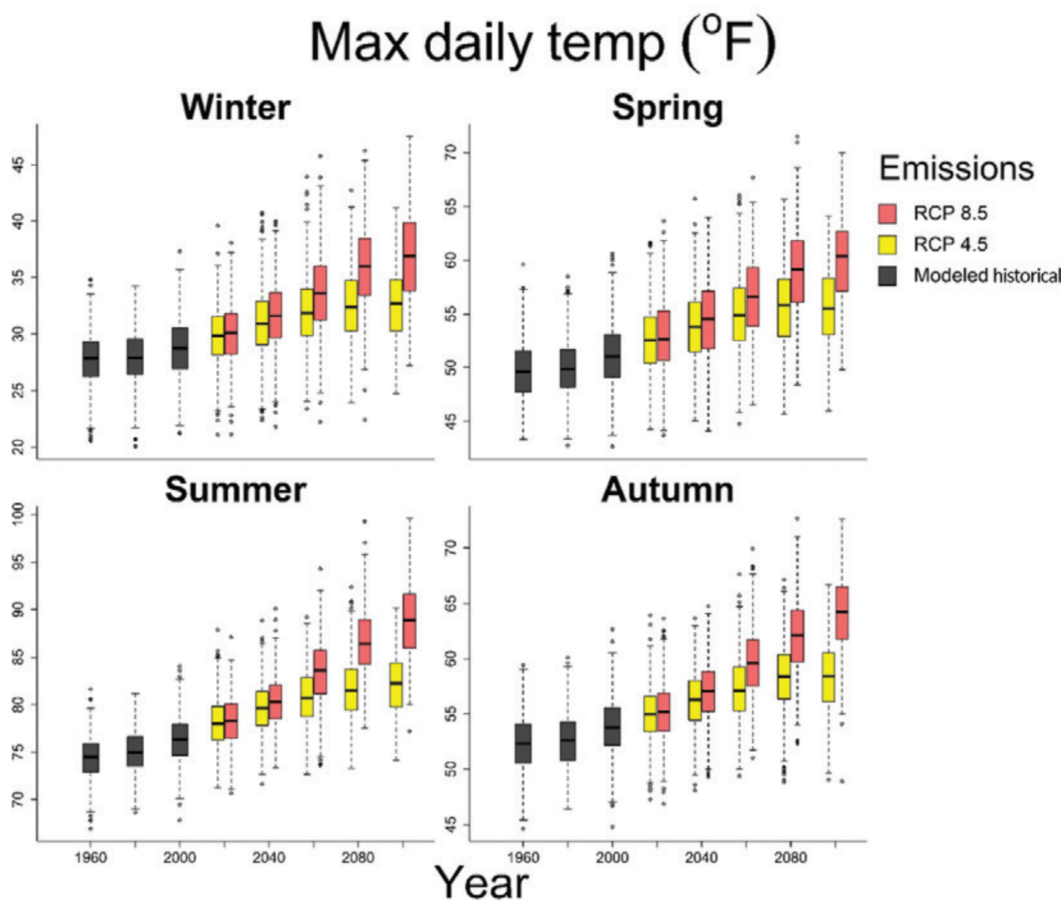

Figure 3.9—Historical modeled and projected seasonal mean monthly maximum temperature for 1950–2100 under RCP 4.5 and RCP 8.5 emissions scenarios for the Middle Rockies subregion of the Intermountain Adaptation Partnership region. See box 3.1 for further explanation.

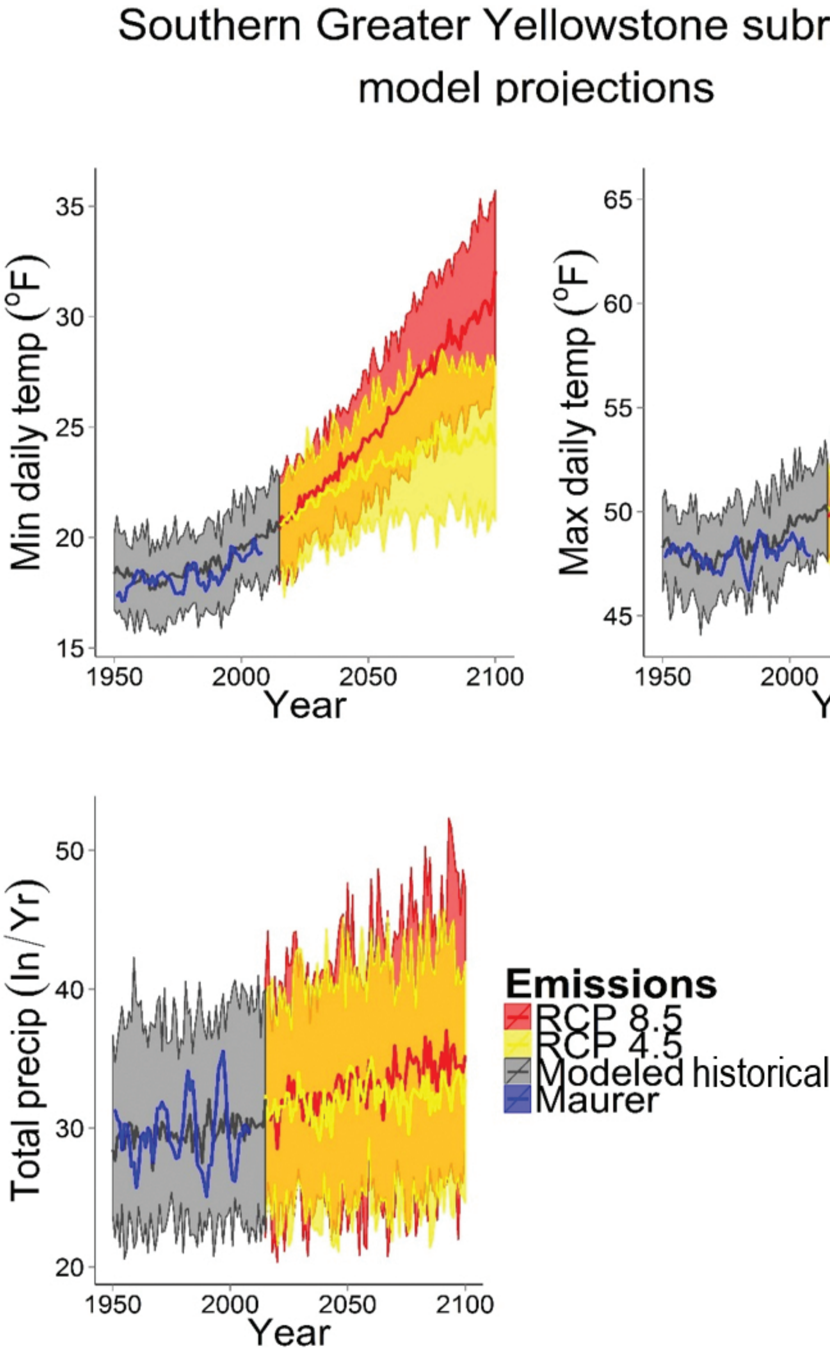

Figure 3.10—Historical modeled and projected annual mean monthly minimum temperature, annual mean monthly maximum temperature, and total annual precipitation for 1950–2100 under RCP 4.5 and RCP 8.5 emissions scenarios based on CMIP5 data for the Southern Greater Yellowstone subregion of the Intermountain Adaptation Partnership region. Historical annual data from the gridded Maurer et al. (2007) dataset are also shown. See box 3.1 for further explanation.

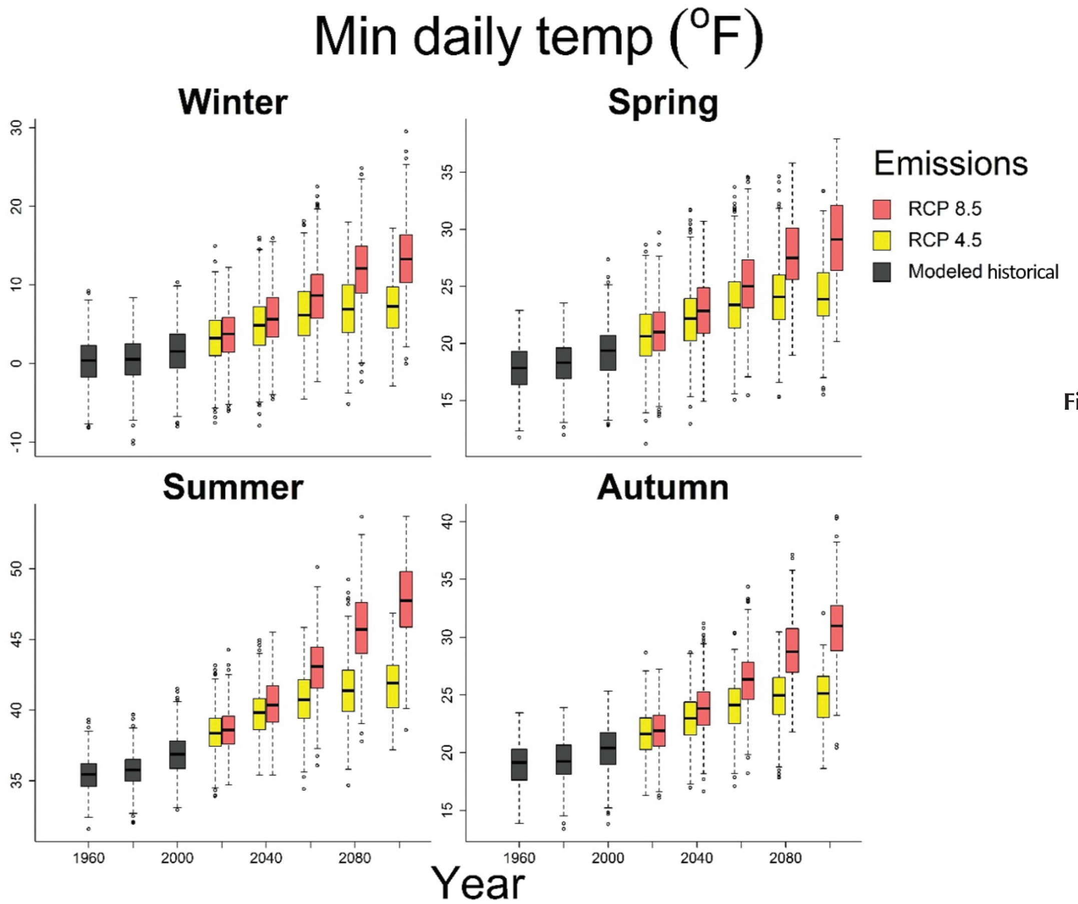

Figure 3.11— Historical modeled and projected seasonal mean monthly minimum temperature for 1950–2100 under RCP 4.5 and RCP 8.5 emissions scenarios for the Southern Greater Yellowstone subregion of the Intermountain Adaptation Partnership region. See box 3.1 for further explanation.

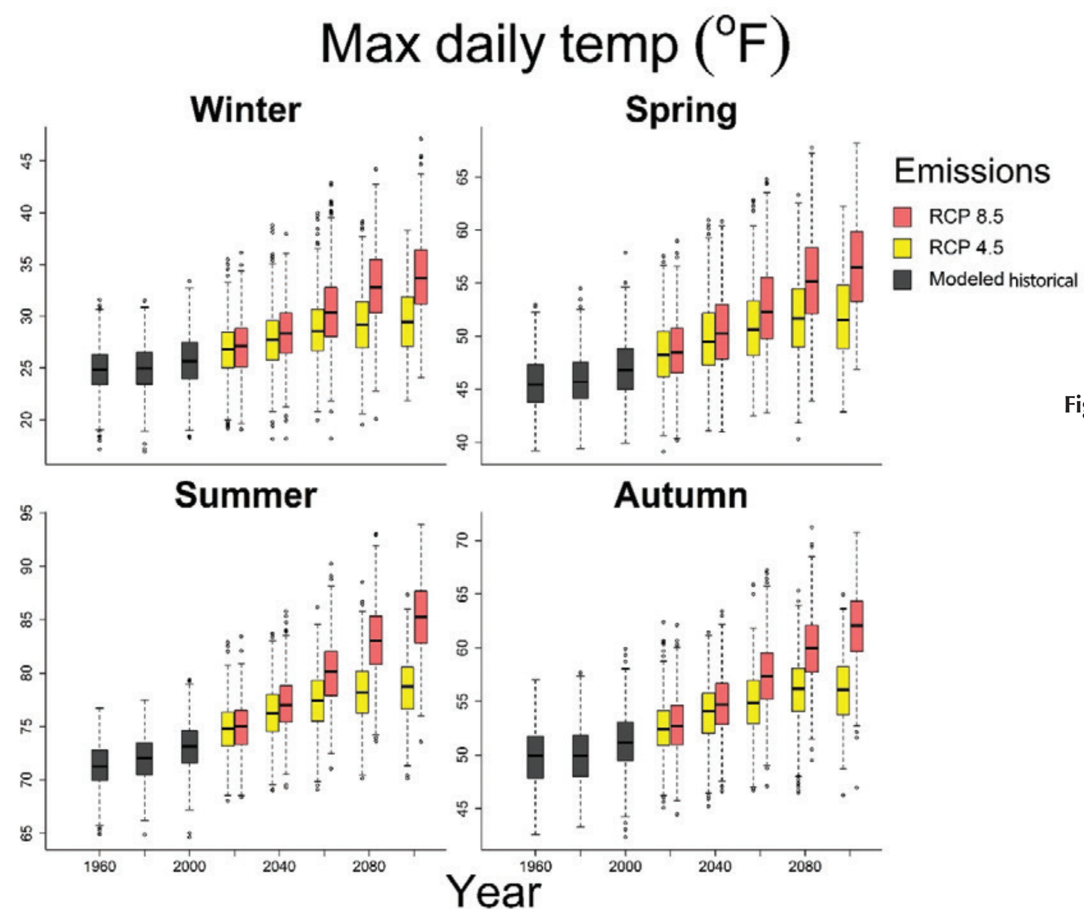

Figure 3.12—Historical modeled and projected seasonal mean monthly maximum temperature for 1950–2100 under RCP 4.5 and RCP 8.5 emissions scenarios for the Southern Greater Yellowstone subregion of the Intermountain Adaptation Partnership region. See box 3.1 for further explanation.

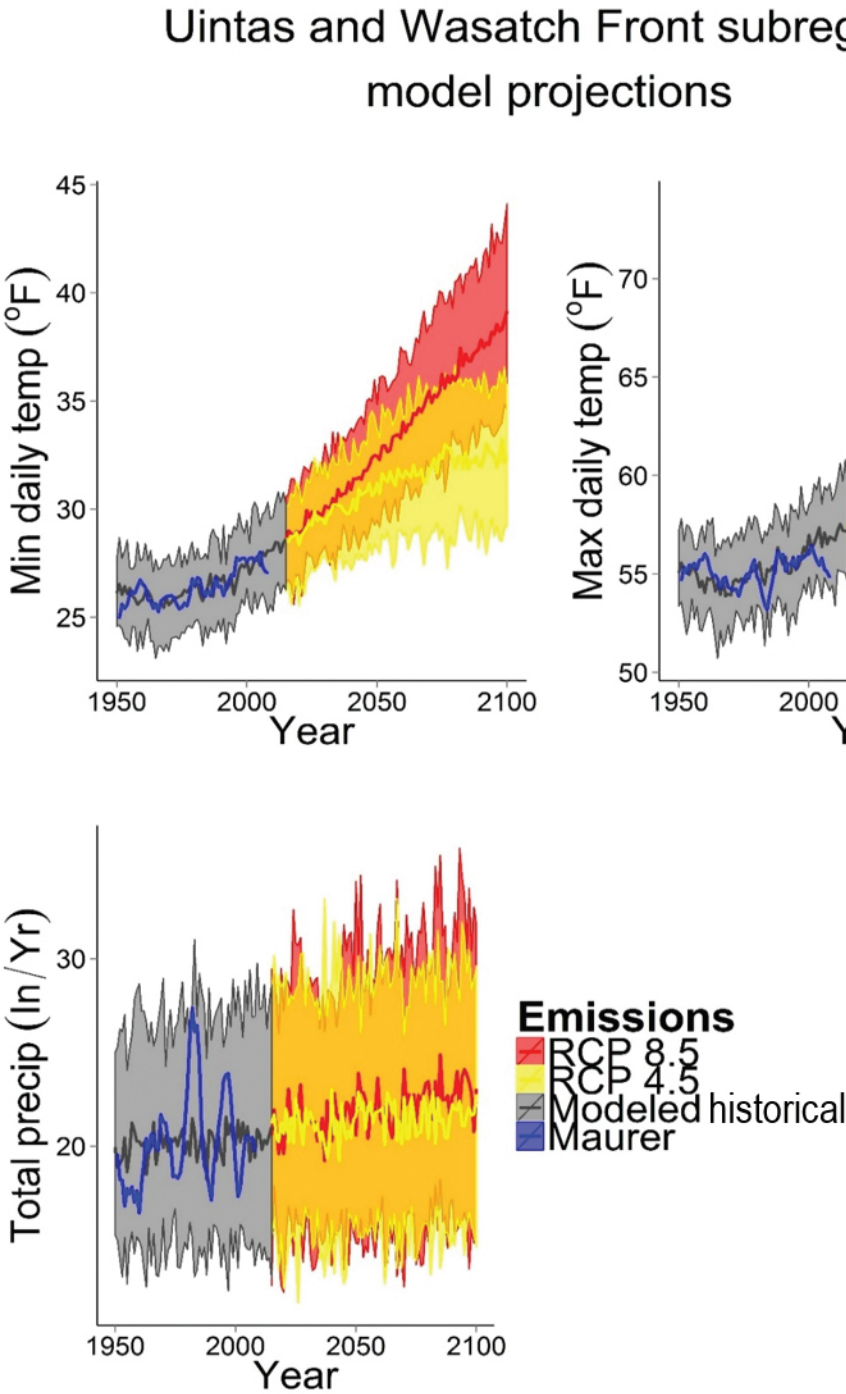

Figure 3.13—Historical modeled and projected annual mean monthly minimum temperature, annual mean monthly maximum temperature, and total annual precipitation for 1950–2100 under RCP 4.5 and RCP 8.5 emissions scenarios based on CMIP5 data for the Uintas and Wasatch Front subregion of the Intermountain Adaptation Partnership region. Historical annual data from the gridded Maurer et al. (2007) dataset are also shown. See box 3.1 for further explanation.

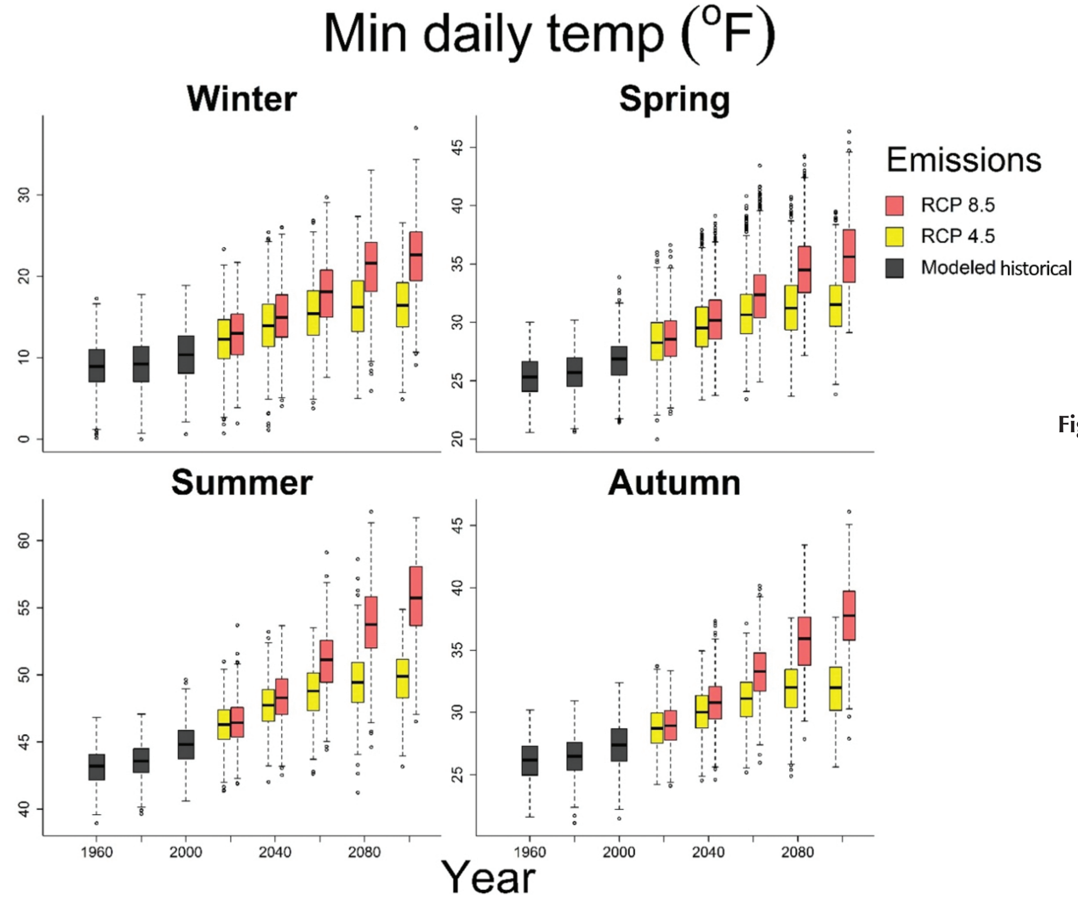

Figure 3.14— Historical modeled and projected seasonal mean monthly minimum temperature for 1950–2100 under RCP 4.5 and RCP 8.5 emissions scenarios for the Uintas and Wasatch Front subregion of the Intermountain Adaptation Partnership region. See box 3.1 for further explanation.

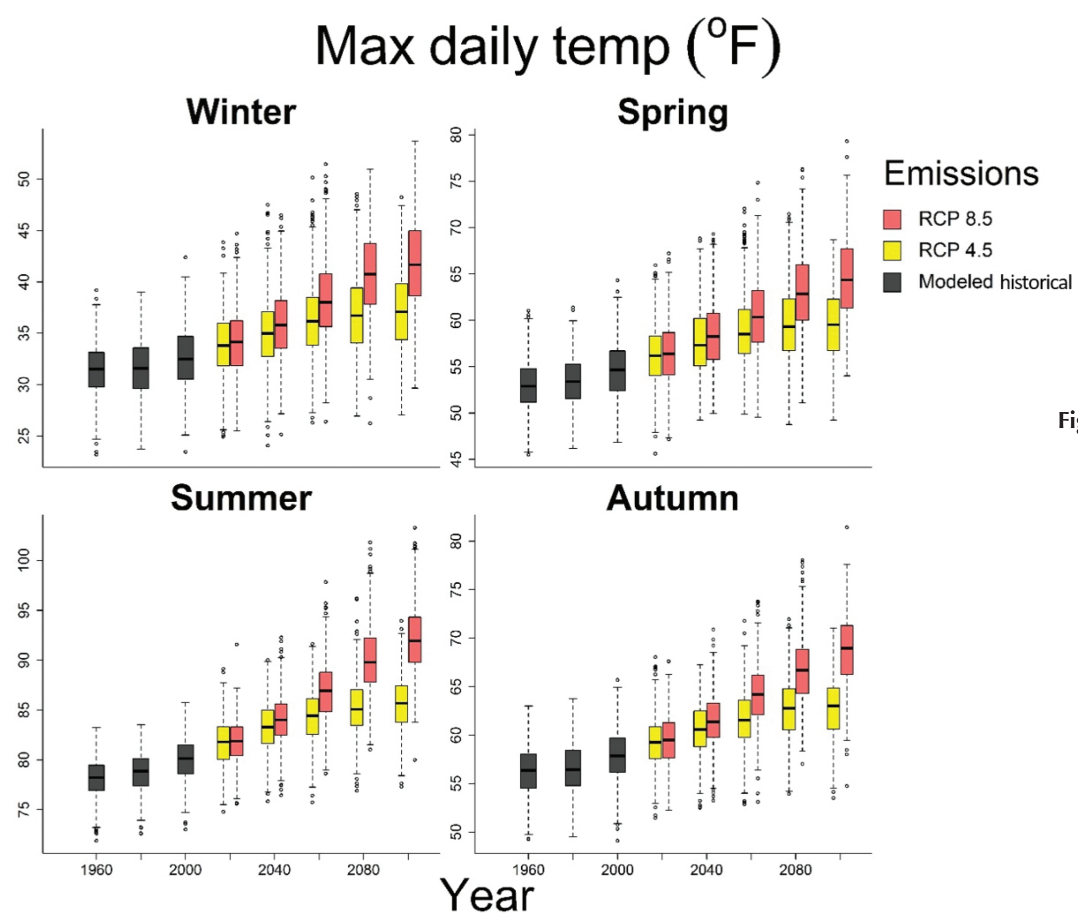

Figure 3.15— Historical modeled and projected seasonal mean monthly maximum temperature for 1950–2100 under RCP 4.5 and RCP 8.5 emissions scenarios for the Uintas and Wasatch Front subregion of the Intermountain Adaptation Partnership region. See box 3.1 for further explanation.

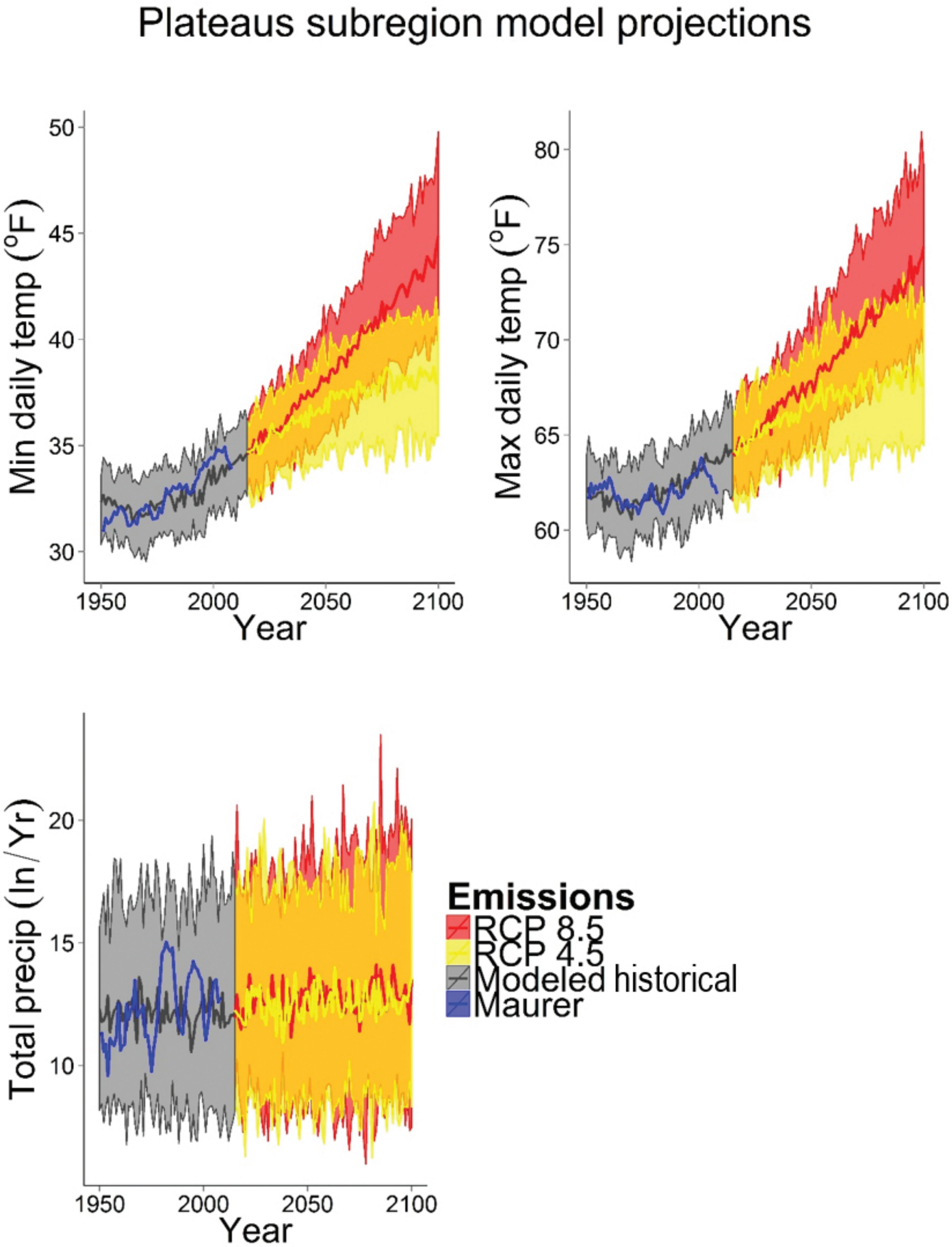

Figure 3.16—Historical modeled and projected annual mean monthly maximum temperature, annual mean monthly minimum temperature, and total annual precipitation for 1950–2100 under RCP 4.5 and RCP 8.5 emissions scenarios based on CMIP5 data for the Plateaus subregion of the Intermountain Adaptation Partnership region. Historical annual data from the gridded Maurer et al. (2007) dataset are also shown. See box 3.1 for further explanation.

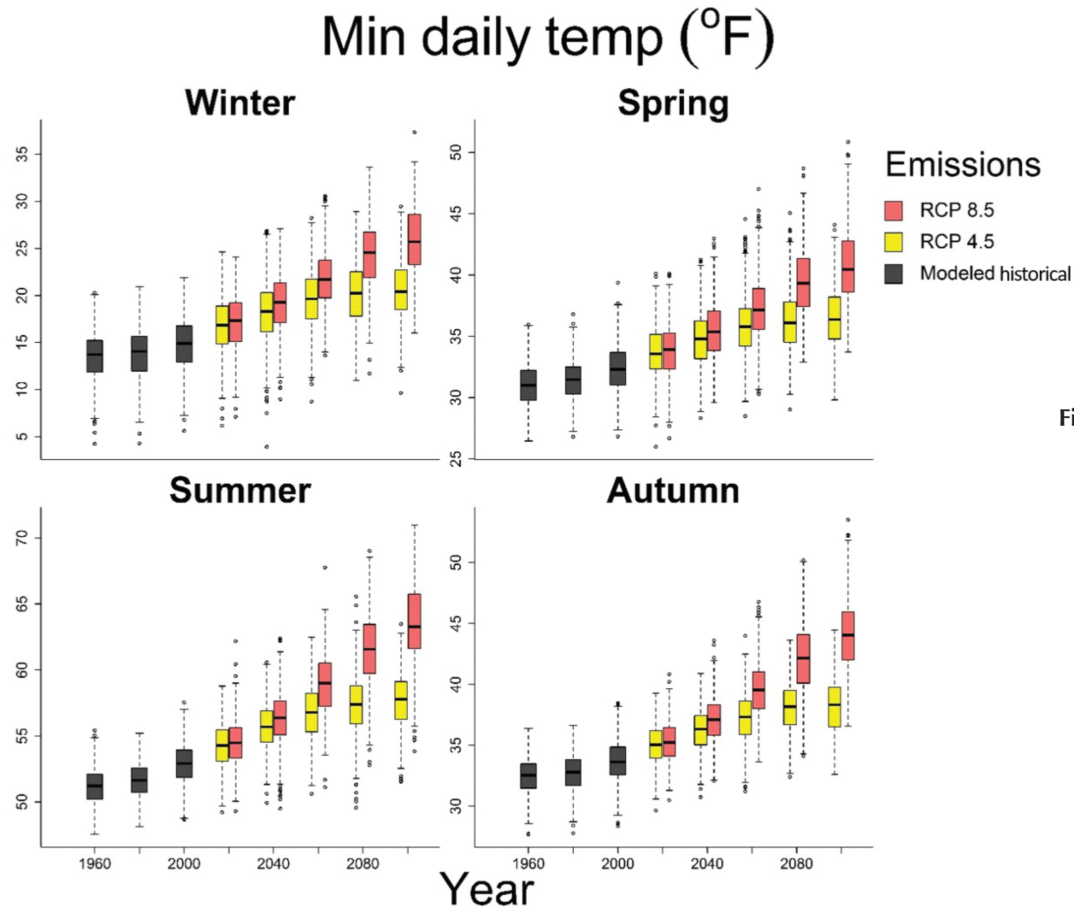

Figure 3.17— Historical modeled and projected seasonal mean monthly minimum temperature for 1950–2100 under RCP 4.5 and RCP 8.5 emissions scenarios for the Plateaus subregion of the Intermountain Adaptation Partnership region. See box 3.1 for further explanation.

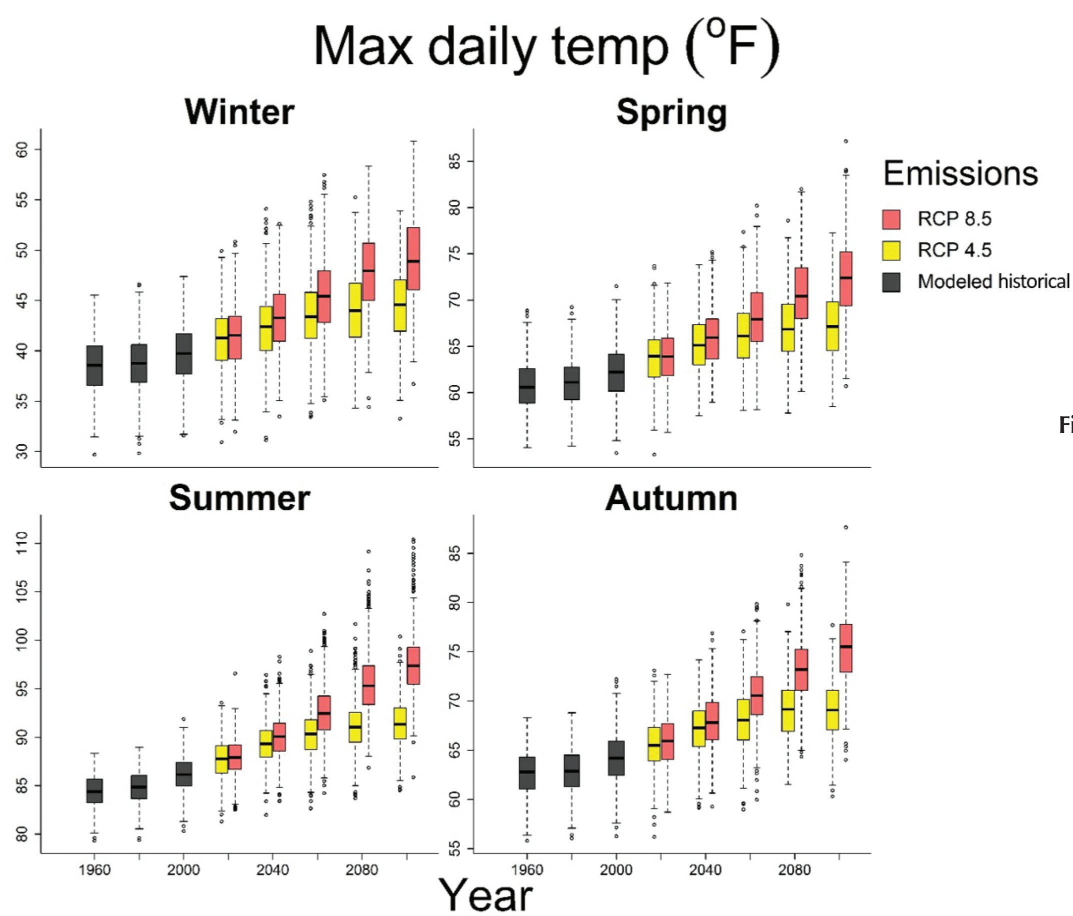

Figure 3.18— Historical modeled and projected seasonal mean monthly maximum temperature for 1950–2100 under RCP 4.5 and RCP 8.5 emissions scenarios for the Plateaus subregion of the Intermountain Adaptation Partnership region. See box 3.1 for further explanation.

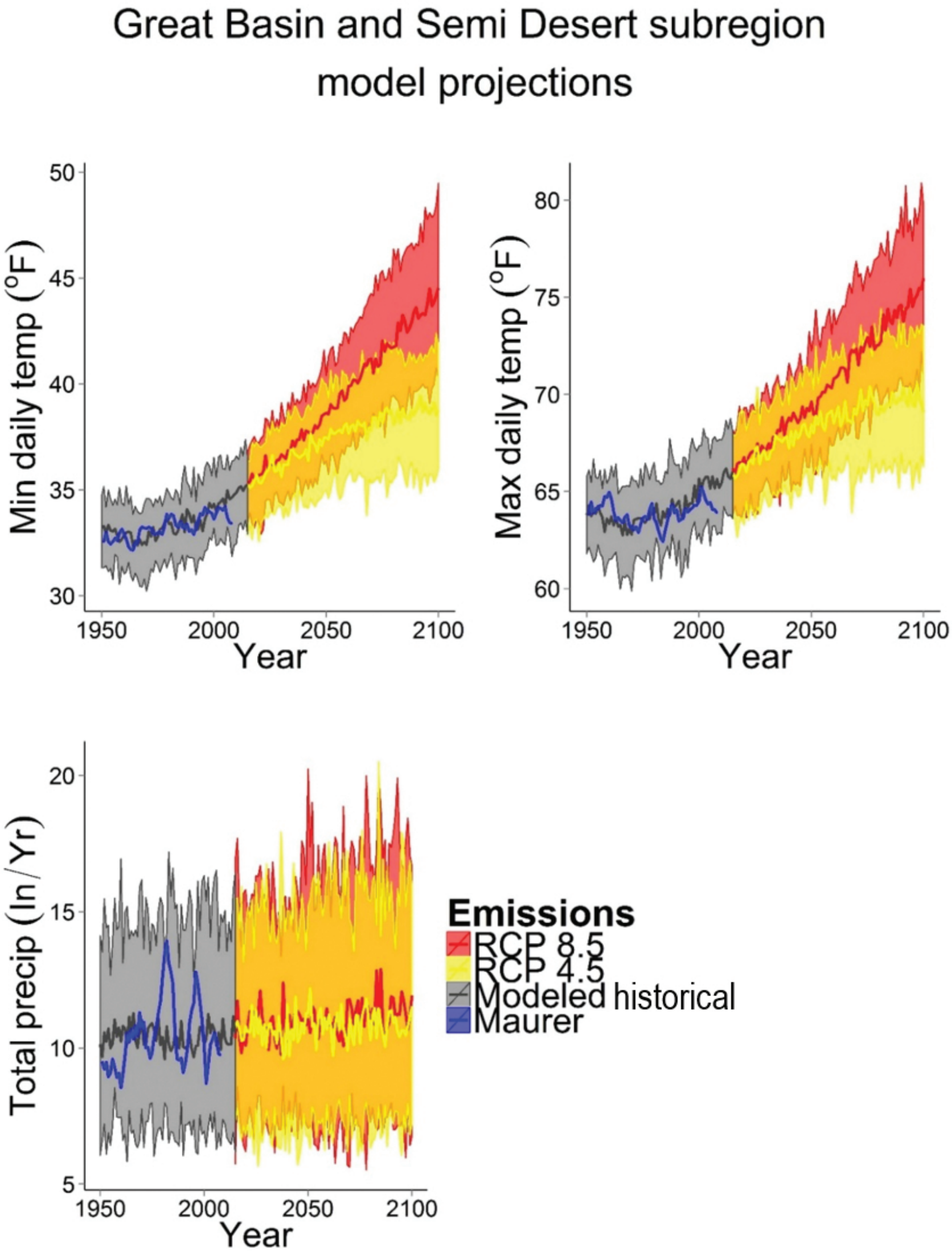

Figure 3.19—Historical modeled and projected annual mean monthly minimum temperature, annual mean monthly maximum temperature, and total annual precipitation for 1950–2100 under RCP 4.5 and RCP 8.5 emissions scenarios based on CMIP5 data for the Great Basin and Semi Desert subregion of the Intermountain Adaptation Partnership region. Historical annual data from the gridded Maurer et al. (2007) dataset are also shown. See box 3.1 for further explanation.

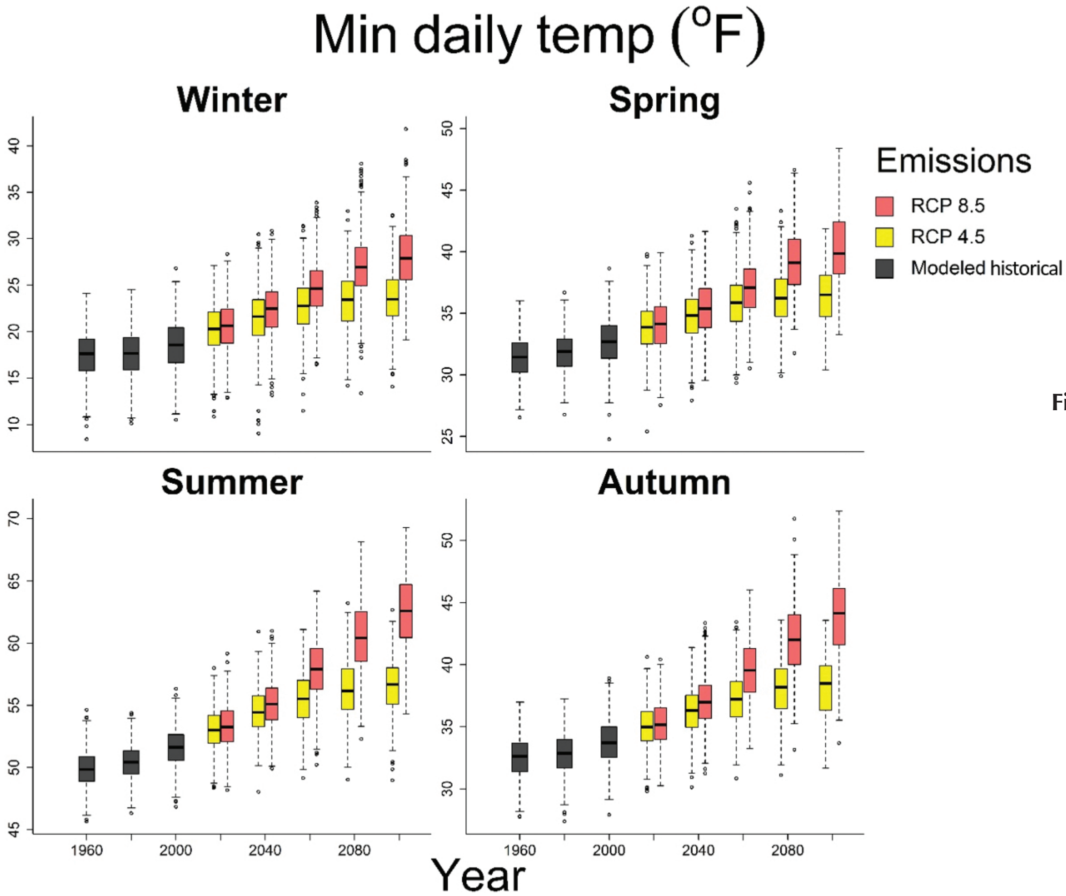

Figure 3.20—Historical modeled and projected seasonal mean monthly minimum temperature for 1950–2100 under RCP 4.5 and RCP 8.5 emissions scenarios for the Great Basin and Semi Desert region of the Intermountain Adaptation Partnership region. See box 3.1 for further explanation.

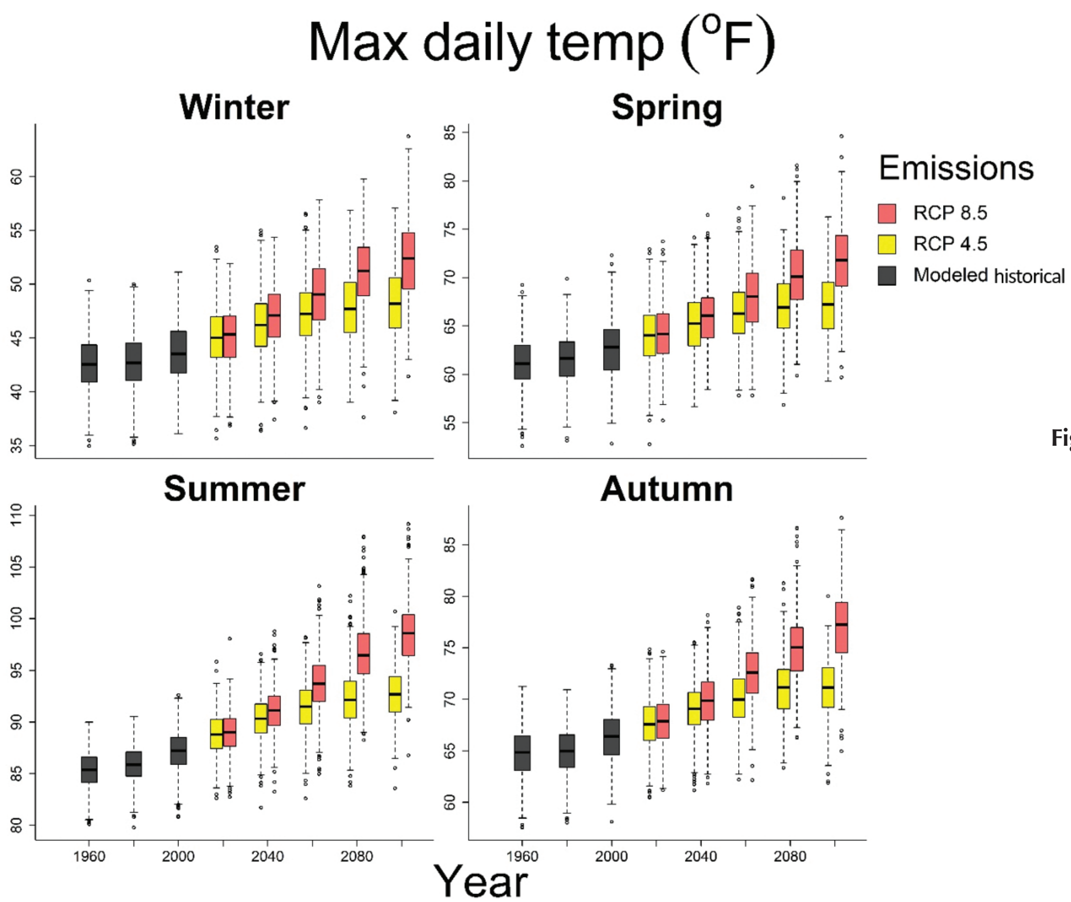

Figure 3.21—Historical modeled and projected seasonal mean monthly maximum temperature for 1950–2100 under RCP 4.5 and RCP 8.5 emissions scenarios for the Great Basin and Semi Desert subregion of the Intermountain Adaptation Partnership region. See box 3.1 for further explanation.

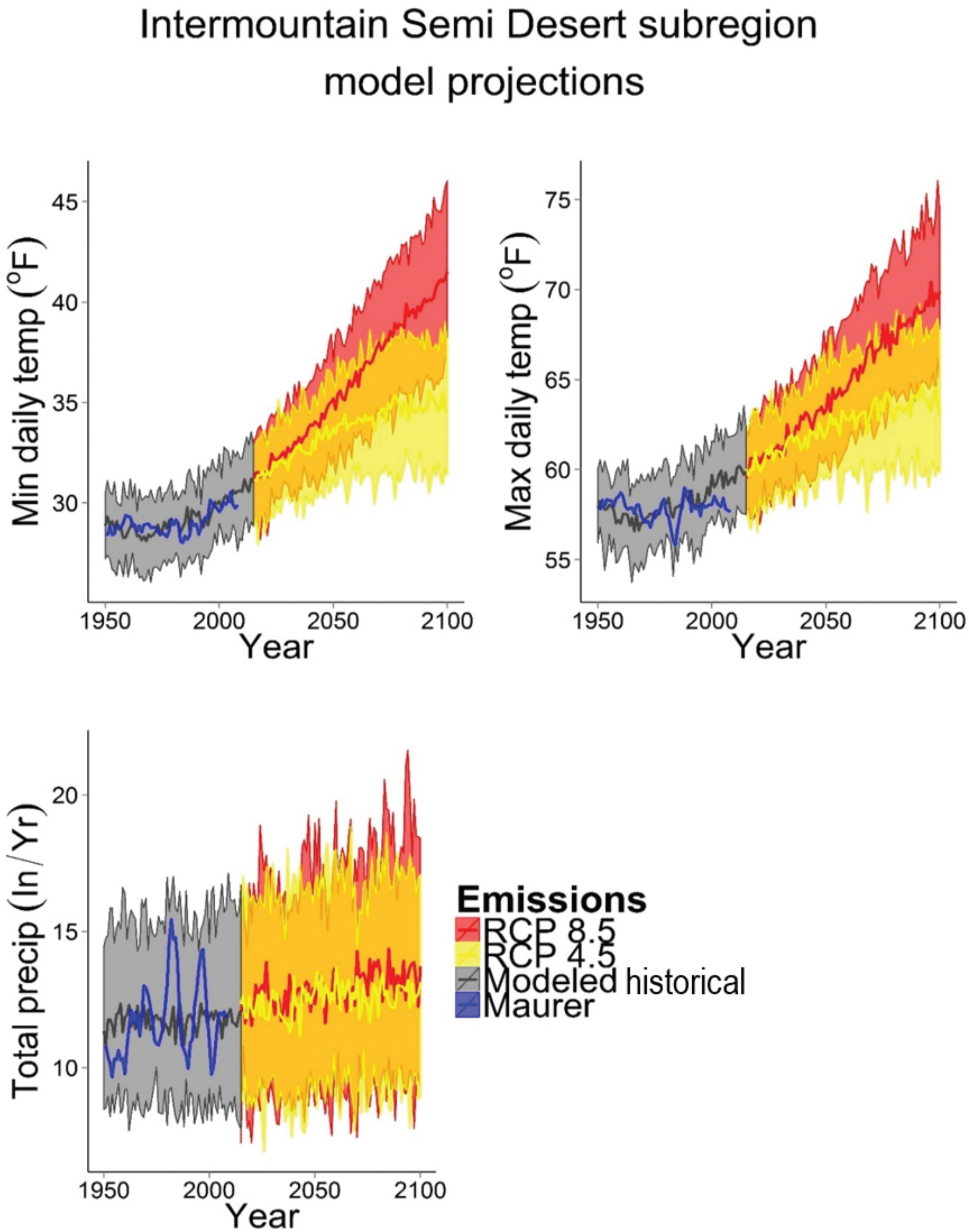

Figure 3.22—Historical modeled and projected annual mean monthly minimum temperature, annual mean monthly maximum temperature, and total annual precipitation for 1950–2100 under RCP 4.5 and RCP 8.5 emissions scenarios based on CMIP5 data for the Intermountain Semi Desert subregion of the Intermountain Adaptation Partnership region. Historical annual data from the gridded Maurer et al. (2007) dataset are also shown. See box 3.1 for further explanation.

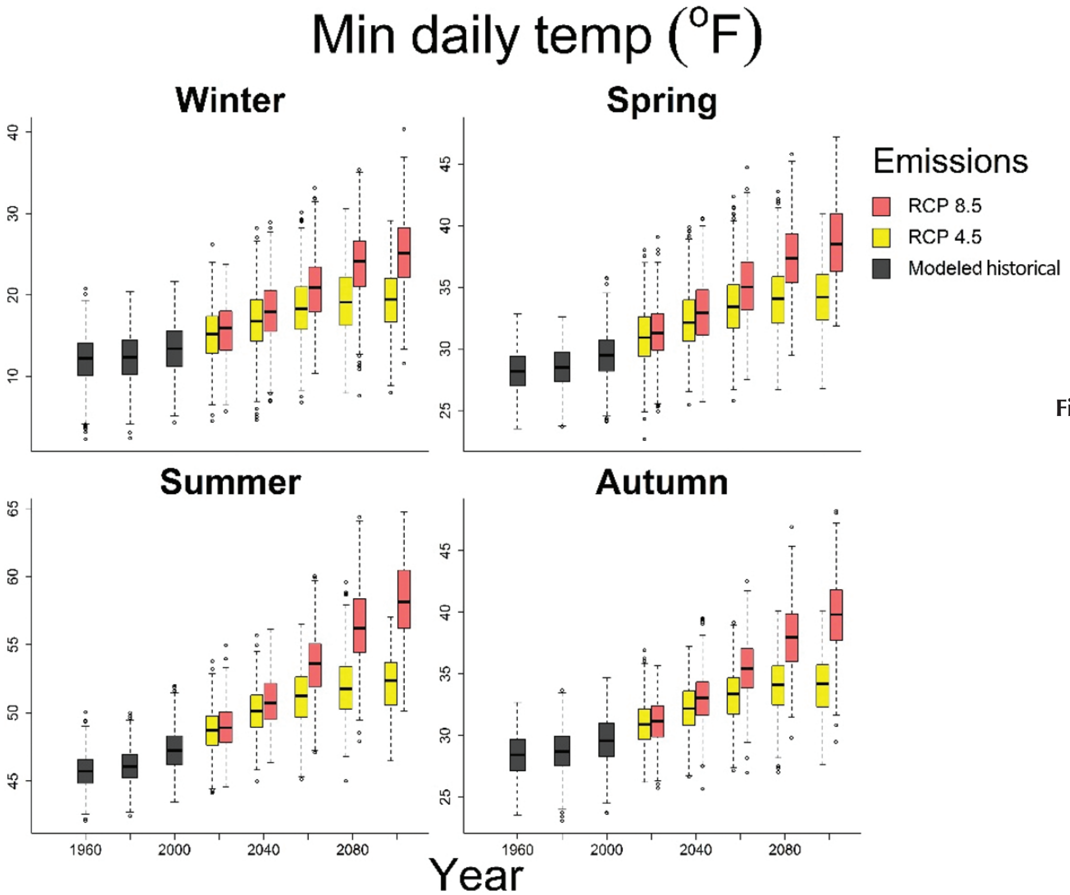

Figure 3.23—Historical modeled and projected seasonal mean monthly minimum temperature for 1950–2100 under RCP 4.5 and RCP 8.5 emissions scenarios for the Intermountain Semi Desert subregion of the Intermountain Adaptation Partnership region. See box 3.1 for further explanation.

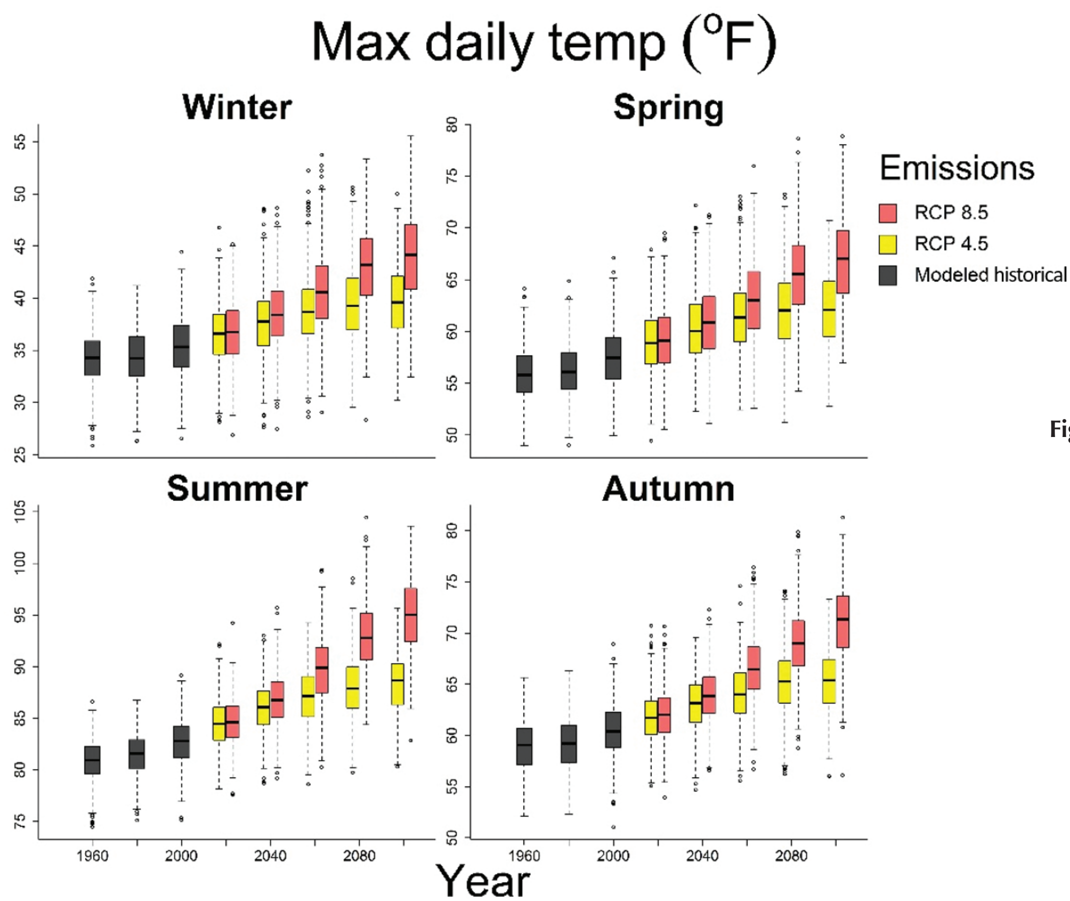

Figure 3.24— Historical modeled and projected seasonal mean monthly maximum temperature for 1950–2100 under RCP 4.5 and RCP 8.5 emissions scenarios for the Intermountain Semi Desert subregion of the Intermountain Adaptation Partnership region. See box 3.1 for further explanation.

References

Andretta, T.A.; Geerts, B. 2010. Heavy snowfall produced by topographically induced winds in the Snake River Plain of Eastern Idaho. Part I: Observational analysis. E-Journal of Severe Storms Meteorology. 5. http://www.ejssm.org/ojs/index.php/ejssm/article/viewArticle/56/74 [Accessed July 13, 2017].

Bekker, M.F.; DeRose, R.J.; Buckley, B.M.; [et al.]. 2014. A 576-year Weber River streamflow reconstruction from tree rings for water resource risk assessment in the Wasatch Front, Utah. Journal of the American Water Resources Association. 50: 1338–1348.

Davey, C.A.; Redmond, K.T.; Simeral, D.B. 2006. Weather and climate inventory, National Park Service, Rocky Mountain Network. Natural Resource Technical Report NPS/GRYN/NRTR—2006/001. Fort Collins, CO: National Park Service. 83 p.

DeRose, R.J.; Bekker, J.F.; Wang, S.-Y.; [et al.]. 2015. A millennium-length reconstruction of Bear River stream flow, Utah. Journal of Hydrology. 529: 524–534.

Gillies, R.R.; Ramsey, R.D. 2009. Climate of Utah. In: Banner, R.E., Baldwin, B.D., Leydsman McGinty, E.K., project coordinators. Rangeland resources of Utah. Logan, UT: Utah State University, Cooperative Extension Service. http://extension.usu.edu/rangelands/ou-files/RRU_Introduction.pdf [Accessed December 5, 2016].

Gillies, R.R.; Wang, S-Y.; Booth, M.R. 2012. Observational and synoptic analyses of the winter precipitation regime change over Utah. Journal of Climate. 25: 4679–4698.

Gray, S.T.; Jackson, S.T.; Betancourt, J.L. 2004. Tree-ring based reconstructions of interannual to decadal scale precipitation variability for northeastern Utah since 1226 A.D. Journal of American Water Resources Association. 40: 947–960.

Hoekema, D.J.; Sridhar, V. 2011. Relating climatic attributes and water resources allocation: A study using surface water supply and soil moisture indices in the Snake River Basin, Idaho. Water Resources Research. 47: W07536. doi:10.1029/2010WR009697.

Houghton, J.T.; Ding, Y.; Griggs, D.J.; [et al.], eds. 2001. Climate change 2001: The scientific basis. Contribution of working group I to the third assessment report of the Intergovernmental Panel on Climate Change. Cambridge, United Kingdom and New York, NY: Cambridge University Press. 881 p.

Intergovernmental Panel on Climate Change Data Distribution Center [IPCC]. 2016. Scenario process of AR5. http://sedac.ipcc-data.org/ddc/ar5_scenario_process/index.html [Accessed March 22, 2017].

Isaak, D.J.; Luce, C.H.; Rieman, B.E.; [et al.]. 2010. Effects of climate change and wildfire on stream temperatures and salmonid thermal habitat in a mountain river network. Ecological Applications. 20: 1350–1371.

Klos, P.Z.; Link, T.E.; Abatzoglou, J.T. 2014. Extent of the rain-snow transition zone in the western U.S. under historic and projected climate. Geophysical Research Letters. 41: 4560–4568.

Kunkel, K.E.; Stevens, L.E.; Stevens, S.E.; [et al.]. 2013. Regional climate trends and scenarios for the U.S. National Climate Assessment: Part 5. Climate of the Southwest U.S. NOAA Technical Report NESDIS 142-5. Washington, DC: National Oceanic and Atmospheric Administration, National Environmental Satellite, Data, and Information Service. 87 p.

Leydsman McGinty, E.I.; McGinty, C.M. 2009. The physiography of Utah. In: Banner, R.E.; Baldwin, B.D.; Leydsman McGinty, E.K., project coordinators. Rangeland resources of Utah. Logan, Utah: Logan, UT: Utah State University, Cooperative Extension Service. http://extension.usu.edu/rangelands/ou-files/RRU_Introduction.pdf [Accessed December 5, 2016].

Littell, J.S.; Elsner, M.M.; Mauger, G.S.; [et al.]. 2011. Regional climate and hydrologic change in the northern US Rockies and Pacific Northwest: internally consistent projections of future climate for resource management. Unpublished project report. http://cses.washington.edu/picea/USFS/pub/Littell_etal_2010 [Accessed December 5, 2016].

Louderback, L.A.; Rhode, D.; Madsen, D.B.; Metcalf, M. 2015. Rapid vegetation shifts in the Uinta Mountains (Utah and Wyoming, USA) during the Late Pleistocene and Holocene. Palaeogeography, Palaeoclimatology, Palaeoecology. 438: 327–343.

MacDonald, G.M.; Tingstad, A.H. 2007. Recent and multicentennial precipitation variability and drought occurrence in the Uinta Mountains region, Utah. Arctic, Antarctic, and Alpine Research. 39: 549–555.

Maurer, E.P.; Wood, A.W.; Adam, J.C.; [et al.]. 2002. A long-term hydrologically based dataset of land surface fluxes and states for the conterminous United States. Journal of Climate. 15: 3237–3251.

Maurer, E.P.; Brekke, L.; Pruitt, T.; Duffy, P.B. 2007. Fine-resolution climate projections enhance regional climate change impact studies. Eos Transactions of the American Geophysical Union. 88: 504.

Meehl, G.A.; Covey, C.; Delworth, T.; [et al.]. 2007. The WCRP CMIP3 multimodel data set. Bulletin of the American Meteorological Society. 88: 1383–1394.

Monahan, W.B.; Fisichelli, N.A. 2014. Climate exposure of US national parks in a new era of change. PloS One. 9: e101302. https://doi.org/10.1371/journal.pone.0101302

Moss, R.; Babiker, W.; Brinkman, S.; [et al.]. 2008. Towards new scenarios for the analysis of emissions, climate change, impacts and response strategies. IPCC Expert Meeting Report. Technical Summary. Geneva, Switzerland: Intergovernmental Panel on Climate Change. 25 p.

Moss, R.H.; Edmonds, J.A.; Hibbard, K.A.; [et al.]. 2010. The next generation of scenarios for climate change research and assessment. Nature. 463: 747.

Morrisette, P.M. 1988. The rising level of the Great Salt Lake: Impacts and adjustments. Bulletin of the American Meteorological Society. 69: 1034–1040.

Nakićenović, N.; Davidson, O.; Davis, G.; [et al.]. 2000. Special report on emissions scenarios: A special report of Working Group III of the Intergovernmental Panel on Climate Change. Cambridge, United Kingdom: Cambridge University Press. 599 p.

Ostlind, E. 2011. The Green River Basin: A natural history. Wheatland, WY: Wyoming State Historical Society. http://www.wyohistory.org/encyclopedia/green-river-basin-natural-history [Accessed December 5, 2016].

Oyler, J.W.; Ballantyne, A.; Jencso, K.; [et al.]. 2015a. Creating a topoclimatic daily air temperature dataset for the conterminous United States using homogenized station data and remotely sensed land skin temperature. International Journal of Climatology. 35: 2258–2279.

Oyler, J.W.; Dobrowski, S.Z.; Ballantyne, A.P.; [et al.]. 2015b. Artificial amplification of warming trends across the mountains of the western United States. Geophysical Research Letters. 42: 153–161.

PRISM Climate Group. 2014. Oregon State University. PRISM 4 km climate data, 2014. http://prism.oregonstate.edu/ [Accessed March 31, 2016].

Rice, J.; Bardsley, T.; Gomben, P.; [et al.]. 2017. Assessment of watershed vulnerability to climate change for the Uinta-Wasatch-Cache and Ashley National Forests, Utah. Gen. Tech. Rep. RMRS-GTR-362. Fort Collins, CO: U.S. Department of Agriculture, Forest Service, Rocky Mountain Research Station. 111 p.

Rogelj, J.; Meinshausen, M.; Knutti, R. 2012. Global warming under old and new scenarios using IPCC climate sensitivity range estimates. Nature Climate Change. 2: 248–253.

Solomon, S.; Qin, D.; Manning, M.; [et al.], eds. 2007. Climate change 2007: The physical science basis. Contribution of Working Group I to the fourth assessment report of the Intergovernmental Panel on Climate Change. Cambridge, UK and New York, NY: Cambridge University Press. 996 p.

Stocker, T.F.; Qin, D.; Plattner, G.-K.; [et al.], eds. 2013. Climate change 2013: The physical science basis. Contribution of Working Group I to the fifth assessment report of the Intergovernmental Panel on Climate Change. Cambridge, UK and New York, NY: Cambridge University Press. 1,535 p.

Svejcar, T.; Angell, R.; James, J. 2016. Spatial and temporal variability in minimum temperature trends in the western U.S. sagebrush steppe. Journal of Arid Environments. 133: 125–133.

van Vuuren, D.P.; Edmonds, J.; Kainuma, M.; [et al.]. 2011. The representative concentration pathways: An overview. Climatic Change. 109: 5–31.

Walsh, J.; Wuebbles, D.; Hayhoe, K.; [et al.]. 2014. Our changing climate. In: Melillo, J.M.; Richmond, T.C.; Yohe, G.W., eds. Climate change impacts in the United States: The Third National Climate Assessment. Washington, DC: U.S. Global Change Research Program. p. 19–67.

Western Regional Climate Center [WRCC]. 2016a. Climate of Idaho. https://wrcc.dri.edu/Climate/narrative_id.php [Accessed November 19, 2016].

Western Regional Climate Center [WRCC]. 2016b. Climate of Nevada. https://wrcc.dri.edu/Climate/narrative_wy.php [Accessed November 19, 2016].

Western Regional Climate Center [WRCC]. 2016c. Climate of Utah. https://wrcc.dri.edu/Climate/narrative_ut.php [Accessed November 19, 2016].

Appendix 2—Models Included in the Climate Analysis for the Intermountain Adaptation Partnership Region

Following are the climate models we used in the Intermountain Adaptation Partnership Region climate analysis, and the institutions that developed them. CMIP5 climate projections for RCP 4.5 and RCP 8.5 scenarios were obtained for these models using the downscaled CMIP3 and CMIP5 climate and hydrology projections archive at: http://gdo-dcp.ucllnl.org/downscaled_cmip_projections. The first model run was selected for this analysis. Model runs were available for both RCP 4.5 and RCP 8.5 scenarios, except for the NASA Goddard Institute for Space Studies models GISS-E2-H-CC and GISS-E2-R-CC.

Institution	Climate model
Commonwealth Scientific and Industrial Research Organization and Bureau of Meteorology, Australia	ACCESS1-0
	ACCESS1-3
Beijing Climate Center, China Meteorological Administration	bcc-csm1-1
Beijing Climate Center, China Meteorological Administration	bcc-csm1-1-m
Canadian Centre for Climate Modelling and Analysis	CanESM2
National Center for Atmospheric Research	CCSM4
Community Earth System Model Contributors	CESM1-BGC
	CESM1-CAM5
Centro Euro-Mediterraneo per i Cambiamenti Climatici	CMCC-CM
Centre National de Recherches Météorologiques/Centre Européen de Recherche et Formation Avancée en Calcul Scientifique	CNRM-CM5
Commonwealth Scientific and Industrial Research Organization, Queensland Climate Change Centre of Excellence	CSIRO-Mk3-6-0
EC-EARTH consortium	EC-EARTH
Laboratory of Numerical Modeling for Atmospheric Sciences and Geophysical Fluid Dynamics, Institute of Atmospheric Physics, Chinese Academy of Sciences, and Center for Earth System Science, Tsinghua University	FGOALS-g2
Laboratory of Numerical Modeling for Atmospheric Sciences and Geophysical Fluid Dynamics, Institute of Atmospheric Physics, Chinese Academy of Sciences, and Center for Earth System Science, Tsinghua University	FGOALS-s2
The First Institute of Oceanography, State Oceanic Administration, China	FIO-ESM
NOAA Geophysical Fluid Dynamics Laboratory	GFDL-CM3
	GFDL-ESM2G
	GFDL-ESM2M
NASA Goddard Institute for Space Studies	GISS-E2-H-CC
	GISS-E2-R
	GISS-E2-R-CC
Met Office Hadley Centre (additional HadGEM2-ES realizations contributed by Instituto Nacional de Pesquisas Espaciais)	HADGEM2-AO
Met Office Hadley Centre (additional HadGEM2-ES realizations contributed by Instituto Nacional de Pesquisas Espaciais)	HADGEM2-CC
Met Office Hadley Centre (additional HadGEM2-ES realizations contributed by Instituto Nacional de Pesquisas Espaciais)	HADGEM2-ES

Institute for Numerical Mathematics	INM-CM4
Institut Pierre-Simon Laplace	IPSL-CM5A-LR
	IPSL-CM5A-MR
	IPSL-CM5B-LR
Japan Agency for Marine-Earth Science and Technology, Atmosphere and Ocean Research Institute (The University of Tokyo), and National Institute for Environmental Studies	MIROC-ESM
	MIROC-ESM-CHEM
Atmosphere and Ocean Research Institute (The University of Tokyo), National Institute for Environmental Studies, and Japan Agency for Marine-Earth Science and Technology	MIROC5
Max Planck Institute for Meteorology (MPI-M)	MPI-ESM-LR
Max Planck Institute for Meteorology (MPI-M)	MPI-ESM-MR
Meteorological Research Institute	MRI-CGCM3
Norwegian Climate Centre	NorESM1-M
Norwegian Climate Centre	MorESM1-ME